A geometrically accommodating heart valve replacement

Sophie C. Hofferberth[1]*, Mossab Y. Saeed[1], Lara Tomholt[2,3], Matheus C. Fernandes [2,4], Christopher Payne[1], Karl Price[1], Gerald R. Marx [5], Jesse J. Esch [5], David W. Brown [5], Jonathan Brown [6], Peter E. Hammer[1], James C. Weaver[2], Elazer R. Edelman [6,7], Pedro J. del Nido[1]*

Affiliations:

[1]Department of Cardiac Surgery, Boston Children's Hospital, Harvard Medical School, Boston, MA 02115, USA

[2]Wyss Institute for Biologically Inspired Engineering, Harvard University, Cambridge, MA 02138, USA

[3]Harvard Graduate School of Design, Harvard University, Cambridge, MA, 02138, USA

[4]John A. Paulson School of Engineering and Applied Sciences, Harvard University, Cambridge, MA, 02138, USA

[5]Department of Cardiology, Boston Children's Hospital, Harvard Medical School, Boston, MA 02115, USA

[6]Biomedical Engineering Center, Institute for Medical Engineering & Science, Massachusetts Institute of Technology, Cambridge, MA 02139, USA

[7]Cardiovascular Division, Department of Medicine, Brigham and Women's Hospital, Harvard Medical School, Boston, MA 02115, USA.

***Corresponding authors:**
Sophie C. Hofferberth, sophie.hofferberth@cardio.chboston.org

Pedro J. del Nido, pedro.delnido@cardio.chboston.org

One-sentence summary: We demonstrate a biomimetic prosthetic heart valve that is size-adaptable to accommodate somatic growth and structural asymmetries within the heart.

ABSTRACT

While congenital heart valve disease has life-threatening consequences that warrant early valve replacement, the development of a growth-accommodating prosthetic valve has remained elusive, and as such, thousands of children continue to face multiple high-risk open-heart operations to replace outgrown valves. Here, we demonstrate a biomimetic prosthetic valve that is size-adjustable to accommodate somatic growth and structural asymmetries within the heart. Inspired by the human venous valve, whose geometry is optimized to preserve functionality across a wide range of constantly varying volume loads and diameters, our geometrically accommodating synthetic bileaflet valve analog exhibits similar adaptability to dimensional and shape changes. Benchtop and acute *in vivo* experiments validated design functionality, and *in vivo* survival studies in a growing animal model demonstrated mechanical valve expansion to accommodate growth. As illustrated in this work, dynamic size adaptability with preservation of unidirectional flow in prosthetic valves thus offers a new paradigm of care for the treatment of heart valve disease.

INTRODUCTION

Some 1.35 million children are born with a congenital heart defect each year worldwide, and ~40,000 in the U.S. alone, disrupting childhood development, families, and communities (*1*). Indeed, the heart is the organ most commonly affected by birth malformations (*2*). In the U.S, an estimated 2.4 million children and adults are currently living with congenital heart disease (*3*), at an annual expense of ~$6 billion (*4*). Heart valve defects account for over 25% of all congenital heart disease (*1, 5*). Congenital malformations appear in all of the four native heart valves, including the semilunar pulmonary and aortic valves, and the atrioventricular mitral and tricuspid valves, though the pulmonary valve is most often affected (*1*). Surgical intervention is thus usually required in the first few years of life in order to restore and maintain long term heart function. While the primary goal of these procedures is to repair the native valve to allow for tissue growth, this strategy is often not feasible or successful (*6*). As such, early valve replacement is inevitable in most children with congenital heart valve defects.

Outcomes of valve replacement, however, remain suboptimal, particularly in young children, irrespective of whether biological cryopreserved human cadaveric donor or bioprosthetic tissue valves, or mechanical valves are placed. Biological valves exhibit accelerated structural deterioration from calcification and likely immune attack (*7, 8*), and mechanical valves bear added risk of life-long and life-threatening thromboembolic complications (*9*). Unfortunately, by design, all currently available prosthetic valves have a fixed functional diameter, and therefore cannot accommodate the growth of a child's heart (*10*). Thus, children with congenital valvular defects face multiple invasive open-heart operations to upsize their fixed-size valve or valved conduit (*11-13*). Today, a child who undergoes valve replacement at less than two years of age will require up to five open-heart operations before reaching adulthood (*14-16*). The morbidity of valve replacement surgery in children is significant, with inherent risk of stroke, rhythm abnormalities, bleeding complications, and

prolonged hospital stay (*12, 13, 16*), moreover, mortality rates range from 2 to 30% (*11, 12, 16*). More recently, stent-mounted tissue valves delivered via a transcatheter approach have emerged as a less invasive alternative for pulmonary valve replacement (*17, 18*). However, these existing devices have limited expansion capacity, and require large diameter delivery systems, which preclude valve implantation in infants and small children (*19*). Furthermore, valve deployment in older children and adolescents is often prohibited by large or asymmetric vessels (*20*).

Many seek a growth-accommodating prosthetic valve, suitable for implantation from infancy through to adulthood. However, this is not a simple matter. Such a device must allow for annular circumference expansion, but without loss of function resulting from energy loss, stenoses and/or regurgitation, or increased wear and tear.

Motivated by these requirements, here we demonstrate a biomimetic balloon-expandable prosthetic heart valve that is size-adjustable to accommodate somatic growth, compensate for structural asymmetries, and even dynamic structural oscillations. The valve design draws inspiration from the geometric profile of the native human venous valve, whose structure is optimized to preserve functionality in the face of marked vicissitudes in transmitted vascular volumes. We closely mimicked the dynamic structure-function relationship of the native venous valve to design a geometrically accommodating valve replacement device that maintains optimal function across a wide range of dimensions. We present the device concept, finite element computer simulation and flow-based *in vitro* analyses, acute *in vivo* studies evaluating function of the primary valve geometry, and *in vivo* survival studies demonstrating proof-of-concept of valve expansion in a growing animal model.

RESULTS

Human vascular valves - structure and function

Though we traditionally associate valves with the heart, the bulk of valves are in fact vascular, and only the atrioventricular valves are truly cardiac, containing myocardium and active contractile tissue structures. The semilunar arterial valves (fig. 1A) are inherently passive and aside from needing to accommodate non-circular shape changes during the cardiac cycle, are relatively fixed in size. The semilunar valve leaflets insert into a fibrous annulus at attachment points (commissures) 120 degrees apart (fig. 1B). The annulus is a semi-rigid ring of tissue that encircles the base of the valve and exhibits minimal change in diameter in loaded and unloaded states (*21, 22*). The aspect ratio of a semilunar valve is ~0.5:1, with an axial height ~half the annulus diameter (fig. 1B), and this is preserved throughout the cardiac cycle as the annulus dimension is relatively unchanged. As the annulus and leaflet dimensions increase with somatic growth (*23*), the aspect ratio is maintained (fig. 1, B and C).

It is evident that the native semilunar valve geometry is not designed for dynamic diametric expansion. Our recent simulation-based study demonstrated non-living material with native semilunar valve geometry achieves <10% diameter increase before loss of valve function ensues (*24*). Since their introduction over half a century ago, bioprosthetic heart valves have traditionally mimicked the trileaflet semilunar valve geometry (*25*), and as such, all existing surgical prostheses are fixed in diameter. Even trileaflet balloon-expandable transcatheter valves have limited capacity for expansion beyond a single nominal diameter (*26*). While the native semilunar valve design may be suitable for many adult patients, a prosthesis with this geometry does not meet the physiologic and anatomic needs of a growing child.

In contrast to the arterial system, the venous system (fig. 1D) not only returns blood to the heart, but also holds 70% of total blood volume and is 30-fold more compliant than arteries

(*27*). As a capacitance reservoir, veins accommodate large changes in blood volume almost instantaneously (i.e. over a period of seconds) to maintain cardiac filling demands (*27, 28*), and in the process modulate their circumference with up to 4-fold change in vessel diameter (fig. 1, E and F). Venous valves operate in this dynamic environment to ensure unidirectional flow with blood volume recruitment, and vessel diameter change without loss of valve competency (fig. 1E). Unlike the semilunar valves, venous valve leaflets do not attach to a fibrous annulus. Rather, the two leaflets attach at the base of a bulbous sinus (the space between the valve leaflet and vein wall), located in a particularly thin region of the vein wall (fig. 1E). The bulbous sinus expands radially outward under hydrostatic load, accounting for most of the vessel expansion at the level of the valve (*29*) (fig. 1E) Moreover, venous valve leaflets are relatively non-compliant, exhibiting minimal change in surface area under load (*30*).

Early anatomic descriptions noted the axial length of a human venous valve is approximately twice the vessel diameter (*31*), which we have also confirmed experimentally (figs. 1E, S1). Under resting conditions, in the closed position, venous valve leaflets coapt, contact each other, over a length corresponding to up to half the vessel diameter (*32*) (fig. 1E). This coaptation reserve allows for continued leaflet contact under increasing volume loading. As the volume increases, the bulbous sinus dilates, pulling the leaflets radially outward, resulting in sac-like expansion along the valve base. Correspondingly, the valve aspect ratio and coaptation length decreases as the radial dimension increases (fig. 1E, Movie S1 - venous valve). The tall, bileaflet geometry, large leaflet surface area, and considerable coaptation reserve enable the venous valve to close effectively over a wide range of diameters to accommodate large changes in blood volume over short timescales (i.e. seconds, fig. 1F) (*33*).

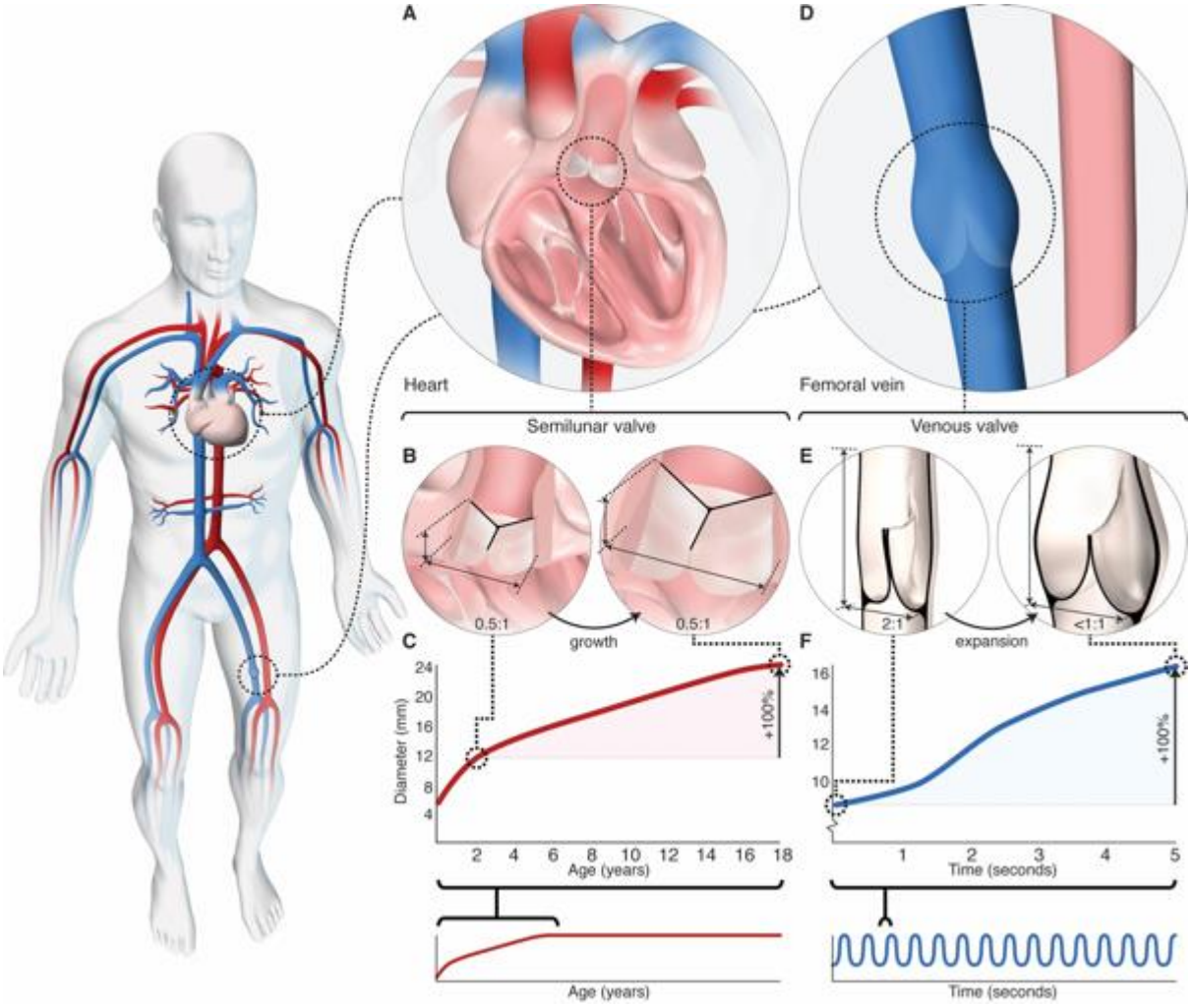

Fig. 1. **Geometry and function of human arterial and venous valves. (A)** Arterial semilunar (pulmonary) valve located within the heart. **(B)** Axial height of human semilunar valve is ~1/2 the annulus diameter and remains constant with growth. **(C)** Semilunar valve (pulmonary) annulus dimension change with somatic growth; ~2-fold increase in diameter between the ages of 2 to 18 years in healthy children (*23*). **(C)** Native venous valve located within vein of lower extremity. **(E)** Leaflet dimensions of human venous valve, at rest. Axial height is ~2 times the vessel diameter and leaflet contact length (coaptation) is up to half the vessel diameter (*30*, *31*). As the vein expands radially with increased volume load, the venous valve aspect ratio decreases (<1:1) and the sinuses dilate to maintain leaflet contact and ensure unidirectional

blood flow. **(F)** Veins accommodate large changes in blood volume almost instantaneously, with up to 4-fold change in vessel diameter over a period of seconds (*33*).

Biomimetic geometrically accommodating heart valve design

Drawing inspiration from the human venous valve, we explored the potential for a geometrically accommodating heart valve design. The fundamental geometric problem that must be overcome by a venous valve is identical to that for any prosthetic valve in a growing child; in both environments the valve must maintain function while accommodating a diametrically expanding orifice. Throughout the course of this study, particular attention was paid to whether we could accommodate the dynamic and evolving dimensional changes imposed by growth by mimicking how the venous valve accounts for dynamic dimensional changes in transmitted ever changing volumes (fig. 2A).

The design of our biomimetic valve centers on three interrelated geometric components, including the leaflet profile geometry, the leaflet attachment geometry, and the valve expansion geometry. The leaflet profile geometry was created based on the morphology and dimensions observed in human venous valve specimens (fig. S1). Key dimensions included the valve axial length, baseline aspect ratio, leaflet mid-height, and leaflet free-edge length (fig. 2A). The leaflet attachment geometry replicated the 3-dimensional geometric curve created by the venous valve leaflet attachment to the surrounding vessel wall (figs. 1D, S1B, 2, Movie S1-venous valve), and is the defining feature of the geometrically accommodating valve design. Finally, we developed a methodology for diametrically expanding the leaflet attachment geometry to achieve radial expansion. To accomplish this, we fixed the length of the 3-dimensional leaflet attachment perimeter, such that radial expansion is accompanied by a reduction in valve height (figs. 2A, S3A). Thus, as the opening diameter increases, the valve

shortens, thereby preserving coaptation without necessitating an increase in leaflet surface area (fig. 2A).

Given the fixed length of the leaflet attachment perimeter, it is the baseline aspect ratio that determines the extent of functional valve expansion, and thereby the extent of growth-accommodation (fig. S3, B and C). Moreover, the baseline aspect ratio may be tailored based on the extent of desired expandability and anatomic constraints (figs. S3C, S4). By combining these critical biomimetic design components, we created a bileaflet valve with a dynamic geometric profile capable of adapting to the anatomic demands of a growing child via mechanical expansion (fig. 2B).

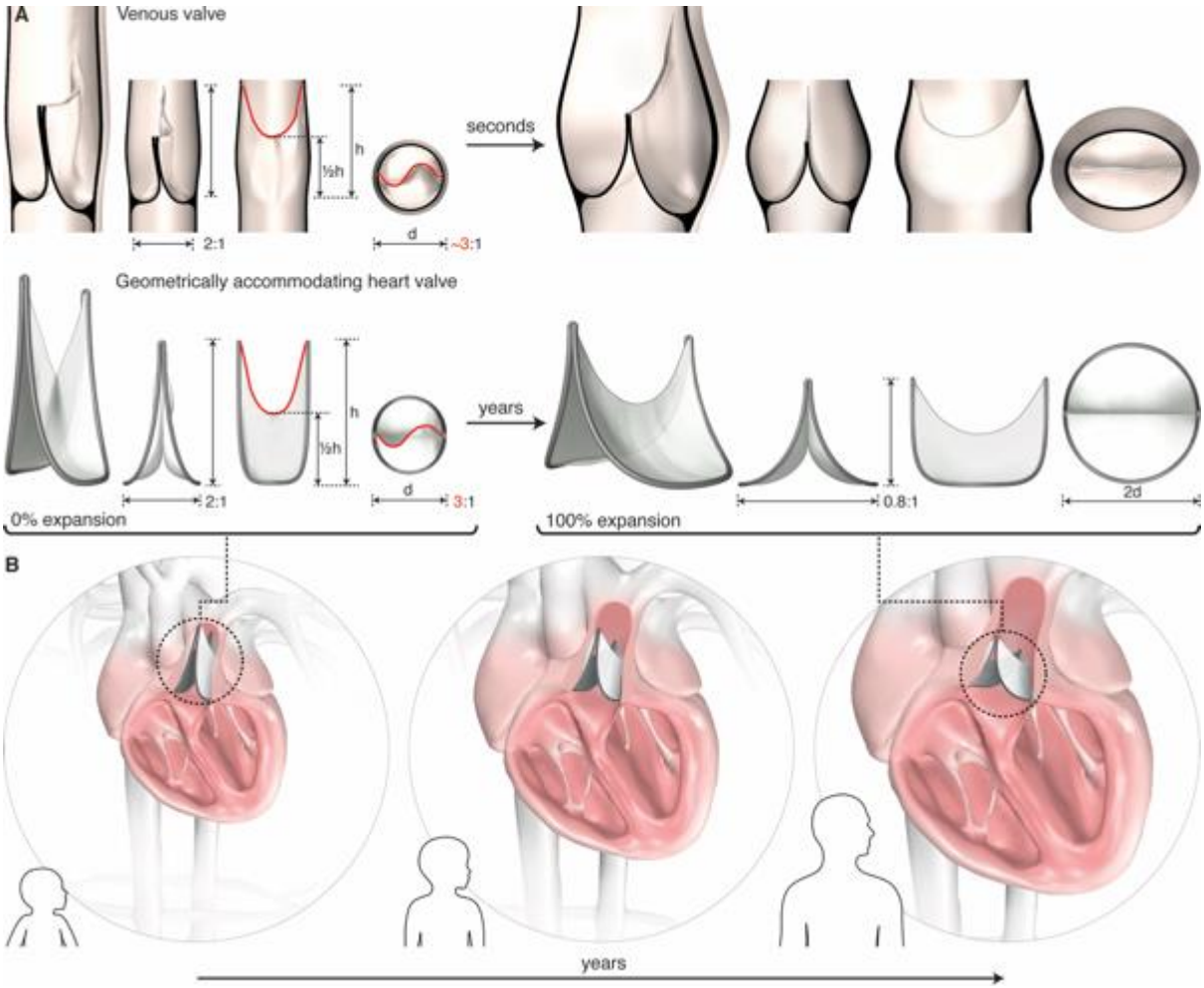

Fig. 2. Design of a biomimetic geometrically accommodating heart valve. (A) Biomimetic valve design inspired by the geometric profile of the human venous valve. Design is defined

by leaflet dimensions, leaflet attachment geometry, and valve expansion geometry. Key leaflet dimensions include the baseline aspect ratio (2:1), leaflet mid-height (1/2h), and free-edge length (red line). The leaflet attachment geometry replicates the 3-dimensional geometric curve created by the venous valve leaflet attachment to the vein wall. The leaflet attachment perimeter is fixed in length, therefore radial expansion is accompanied by a reduction in valve height (aspect ratio decreases to 0.8:1 at 2X expansion). **(B)** Schematic representation of the dynamic biomimetic valve geometry as it adapts to the increasing heart dimensions of a growing child via periodic mechanical balloon expansion.

Primary biomimetic valve geometry - *in vitro* characterization

Benchtop testing examined how the varying aspect ratio of our stent design could achieve radial expansion without compromising valve function. We chose 0.1 mm ePTFE (Goretex, W.L Gore and Associates, Inc., Arizona, USA) as the model leaflet material due to its limited compliance, ease of handling for prototyping purposes, proven clinical track record (*34*), and because its thin membrane and mechanical properties resemble the thin, inelastic native venous valve leaflet (*29*) (fig. S5).

Using this material, we fabricated a series of valve prototypes at different states of diametric expansion, based on the proposed leaflet attachment and leaflet profile geometries (fig. S6). An *in vitro* circulatory flow loop system (fig. S7) was then utilized to define efficiency of forward flow and coaptation (closing function) across a range of expansion states (1X to 1.8X) (fig. 3A, B).

Using adjusted pressure and flow conditions to simulate the dynamic physiology of a growing child, we observed minimal pressure drop (fig. 3A) and physiologic flow profiles (figs. 3B, S8) across all valve expansion states, thus demonstrating the biomimetic valve design enables unobstructed forward flow over a wide range of vessel sizes and flow rates. As

expected, leaflet deformation in the closed state did depend on the degree of expansion and pressure condition, but not at the expense of coaptation. Coaptation under dynamic right and left heart loading conditions well exceeded industry standards (ISO 5840-2:2015) across all valve expansion geometries (fig. 3C). Valve closing function was also not dependent on cycle rate, demonstrating that this leaflet geometry does not display inertial effects, which theoretically could inhibit valve closure in hyperdynamic physiological states, such as in a young child with a rapid heart rate.

To understand leaflet deformation and its stress distribution, we constructed a finite element (FE) model of the expanding valve leaflet in a quasi-static loaded state, under right (fig. 3D, fig. S9) and left heart diastolic loading conditions (fig. S9). Maximum leaflet stresses were at least a factor of 30 below the failure stress of 0.1 mm ePTFE (Goretex) for all valve expansion states and loading conditions. We also repeated the same analysis at smaller, pediatric-specific valve sizes, and found the highest stress values were further reduced by >40% (fig. S10). Notably, there were no areas of stress concentration along the leaflet-frame interface, or elsewhere across the leaflet surface. The lowest stress regions were located at the leaflet commissures (where leaflets meet and insert into the frame) and along the leaflet free edge (region of leaflet contact) (fig. 3D). The pattern of stress distribution is important for the life cycle of a heart valve device, since the presence of localized, high stress regions in trileaflet bioprosthetic valves has been associated with early device failure (*35, 36*). Furthermore, compression and bending of redundant tissue in trileaflet designs leads to alternating negative and positive stress values, which likely induces earlier valve deterioration (*35, 37, 38*). This pattern is not observed in the bileaflet valve geometry (figs. 3D, S9). Thus, the favorable stress/strain profile of our biomimetic bileaflet valve design likely has important implications for long-term device durability.

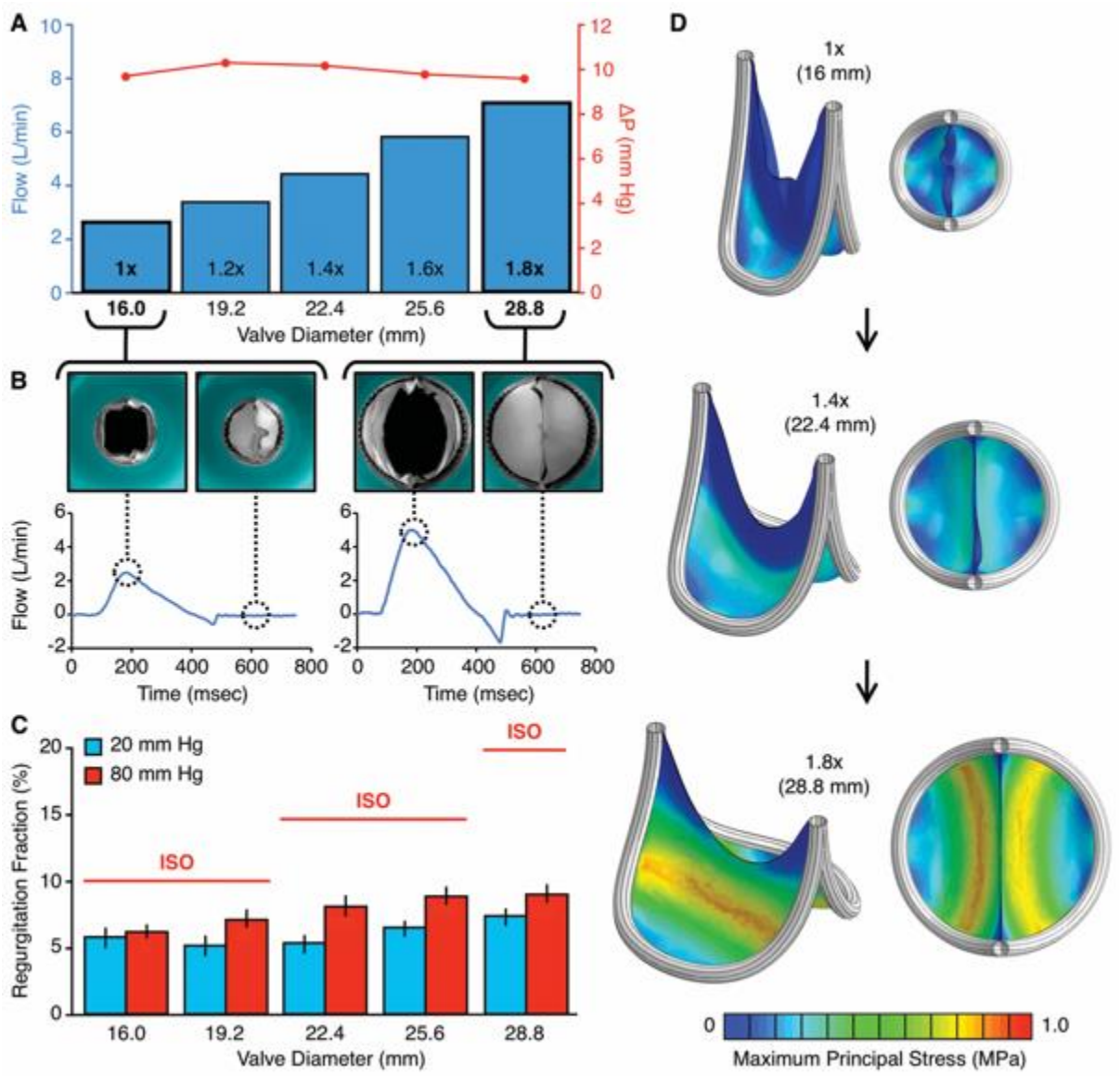

Fig. 3. ***In vitro*** **characterization of the biomimetic bileaflet valve: flow loop testing and computational modeling. (A, B, C)** Valve prototypes tested at different states of diametric expansion (1X to 1.8X) in an *in vitro* circulatory flow loop, under physiologic left and right heart conditions. **(A)** Transvalvular (⊗P) pressure gradient (red line) at each stage of valve expansion (1X to 1.8X). Flow adjusted to match valve size and growing child physiology. **(B)** Top view images of 1X and 1.8X expanded valves within *in vitro* flow loop system, with leaflets in open (left) and closed (right) position, with their corresponding plots demonstrating flow profiles of the 1X and 1.8X expanded valve geometries. **(C)** Leaflet coaptation (closing function) under right (20 mmHg, blue bars) and left (80 mmHg, red bars) heart loads. Error

bars represent ± 1 standard deviation. Red horizontal lines indicate the upper bound industry standard (International Standards Organization; ISO 5840-2:2015) for prosthetic valve regurgitation % under left heart loads. **(D)** Finite element model of leaflet stresses in quasi-static loaded state. Leaflet material is 0.1 mm thickness ePTFE (Goretex), and the results shown are simulated under right heart (20 mmHg) loads. All plots presented are based on the same scale of maximum principal stress, ranging between 0 to 1 MPa.

Primary biomimetic valve geometry - *in vivo* validation

To validate valve performance in an *in vivo* environment, an acute large animal model was established using the two polar expansion states (1X and 1.8X). To match the state of valve expansion to the relevant physiologic environment, fabricated prototypes were implanted in the native pulmonary valve position of juvenile (1X geometry, N = 4) and adult (1.8X geometry, N = 4) sheep (fig. 4, a and b). Valves were implanted using standard surgical techniques (See Supplementary Materials), and the animals were observed for 4 - 6 hours. In all animals, using both geometric configurations, valve hemodynamic performance remained ideal, with trivial transvalvular gradient (pressure drop) (figs. 4, C and D, S11, Tables S2, S3) and physiologic flow profiles (figs. 4, E and F, S11). Color Doppler images obtained via epicardial echocardiogram demonstrated laminar flow along the length of the valve and into the branch pulmonary arteries (Movie S1 - Primary biomimetic valve geometry). Valve coaptation was effective with no significant leakage (fig 4, E and F) observed in any of the eight animal studies (fig. S11, Tables S4, S5). Representative echocardiographic imaging (fig. 4, G and H, Movie S1 - Primary biomimetic valve geometry) confirms these observations and the change in leaflet coaptation length from baseline to complete expansion. For proof-of-principle, the biomimetic valve was implanted in the native aortic valve position of juvenile sheep, demonstrating equivalent mechanical and hemodynamic performance, with

unobstructed forward flow and preserved leaflet coaptation at each stage of valve expansion (See Supplementary Materials, Fig. S12).

These experiments validated our benchtop results and demonstrated proof-of-concept *in vivo*. The consistency of valve function over a wide range of hemodynamic conditions and expansion states highlights the versatility of the biomimetic bileaflet valve design. The kinematic profile of the leaflet attachment geometry is crucial to valve adaptability, since the decrease in valve height with radial expansion preserves the U-shaped geometry of the leaflet free edge (fig. 2B), which serves to retain optimal leaflet mobility across all expansion states (See Movie S1 - primary biomimetic valve expansion). Preserved leaflet mobility thus enables the effective orifice area to increase commensurate with valve diameter and obviates the risk of flow stasis at the valve base.

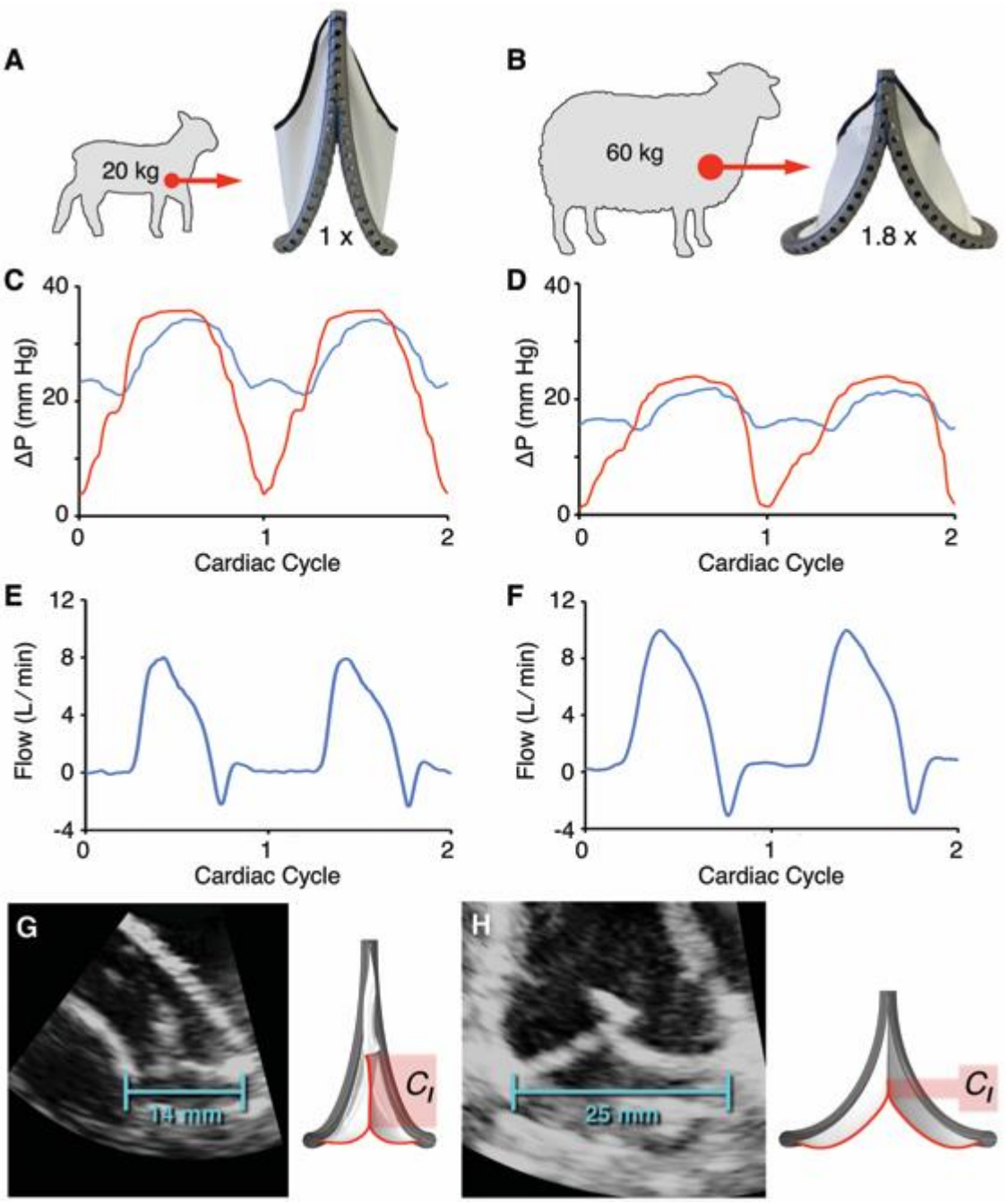

Fig. 4. ***In vivo*** **validation of primary biomimetic valve function: acute studies in juvenile and adult sheep. (A** and **B)** Fabricated prototypes implanted at two polar expansion states (1X and 1.8X) in the native pulmonary valve position of juvenile (N = 4) and adult (N = 4) sheep. **(C** and **D)** Representative plots showing transvalvular (⊗P) pressure gradient for the 1X and 1.8X valve geometries, respectively. RV = right ventricular, PA = pulmonary artery. (**E** and **F**) Corresponding pulmonary artery flow for the 1X and 1.8X valve geometries, respectively. (**G**

and **H**) Representative echocardiographic images of implanted valves, demonstrating change in coaptation length (C_l) between the baseline (1X, 14 mm ID) and fully expanded (1.8X, 25 mm ID) geometries.

Expandable biomimetic valve prototype - *in vitro* design validation and *in vivo* proof-of concept in a growing lamb model

To construct an expandable biomimetic valve prototype, circumferential restraining struts were added to optimize structural support and kinematic profile of the leaflet attachment geometry, while maintaining device symmetry and concentricity (fig. 5, A to D). The geometry, path length, and critically, the location of these support features may be modulated to achieve a circular, out-of-round, or asymmetric expansion profile.

Prototypes were fabricated from 0.1 mm thickness ePTFE leaflets hand-sewn to a laser-cut stainless-steel stent (fig. S13). Valves were tested in an *in vitro* circulatory flow loop system (fig. S7), under simulated pediatric-specific hydrodynamic conditions (ISO 5840-2:2015). Akin to the primary valve geometry, the expandable prototype displayed excellent forward flow efficiency (fig. 5e, fig. S14), with trivial pressure drop (fig. S14) and a >4-fold increase in effective orifice area from 1X to 1.8X diameter expansion (fig. S14). Notably, the indexed effective orifice area (valve diameter/body surface area) increased with progressive valve expansion from 1X to 1.8X (fig. S14), thus indicating that the area of valve opening is preserved along the full length of the leaflet, from the proximal valve opening to the distal leaflet free edge. This geometric feature enables the expandable biomimetic bileaflet valve to maintain optimal forward flow across a wide range of diameters. Moreover, the expandable prototype design maintained effective coaptation along the full length of the leaflet free edge across all expansion states (1X to 1.84X), under both right and left heart diastolic loads (fig. 5e, S14).

Motivated by these benchtop results, we next investigated proof-of-concept *in vivo* device expansion in the face of somatic growth in lambs. Expandable biomimetic valve prototypes were implanted in the native pulmonary valve position of seven juvenile sheep (mean weight = 22.5 ± 0.9 kg, mean age = 9 ± 3 weeks). Implanted valves were expanded via transcatheter balloon dilation at three separate time points over a 9-10 week survival period (See Supplementary Materials). The animals received subcutaneous heparin twice daily for only five days after valve implantation, and for two days after each balloon expansion. There was no chronic anticoagulant or antiplatelet therapy administered. Lambs followed expected growth profiles, gaining >60% in body weight (mean weight at term = 36.7 ± 3.5kg), and their prosthetic valve achieved a 1.6X (20 mm ID) diametric expansion (fig. 5F). In all animals, valve expansions were atraumatic, uniform and symmetric (fig. 5E, F), and there was no elastic recoil of the frame post dilation. Notably, kinematics of the leaflet attachment geometry over 2.5 months of *in vivo* implantation and multiple balloon dilations (fig. 5F) followed exactly what was modeled computationally and observed in our benchtop experiments (fig. 3, fig. S13). Leaflet mobility and coaptation were preserved to achieve unidirectional pulmonary blood flow at all expansion states (See Movie S1-representative 2-D echocardiogram color doppler images). Forward flow efficiency was maintained as the expanding valve orifice matched the hemodynamic demands of the growing lamb (fig. 5G, Table S6, 7). Cardiac catheterization demonstrated intact right ventricular function, low transvalvular pressure gradients and commensurate increase in cardiac output as the valve was expanded up to 1.6X diameter. Serial 2-D transthoracic echocardiogram with continuous wave Doppler demonstrated parabolic flow profiles, with low transvalvular flow velocity at each stage of valve expansion from 12.5 mm to 20 mm ID (fig. S15). This data highlights the absence of functional stenosis with valve diametric expansion. Comprehensive hemodynamic data are presented in Supplemental Materials, Tables 6 and 7. At term, six of the seven animals showed no evidence of valve

regurgitation, and one animal had trivial to mild regurgitation, based on angiographic and echocardiographic imaging (See Movie S1 - Expandable biomimetic valve geometry, fig. S15).

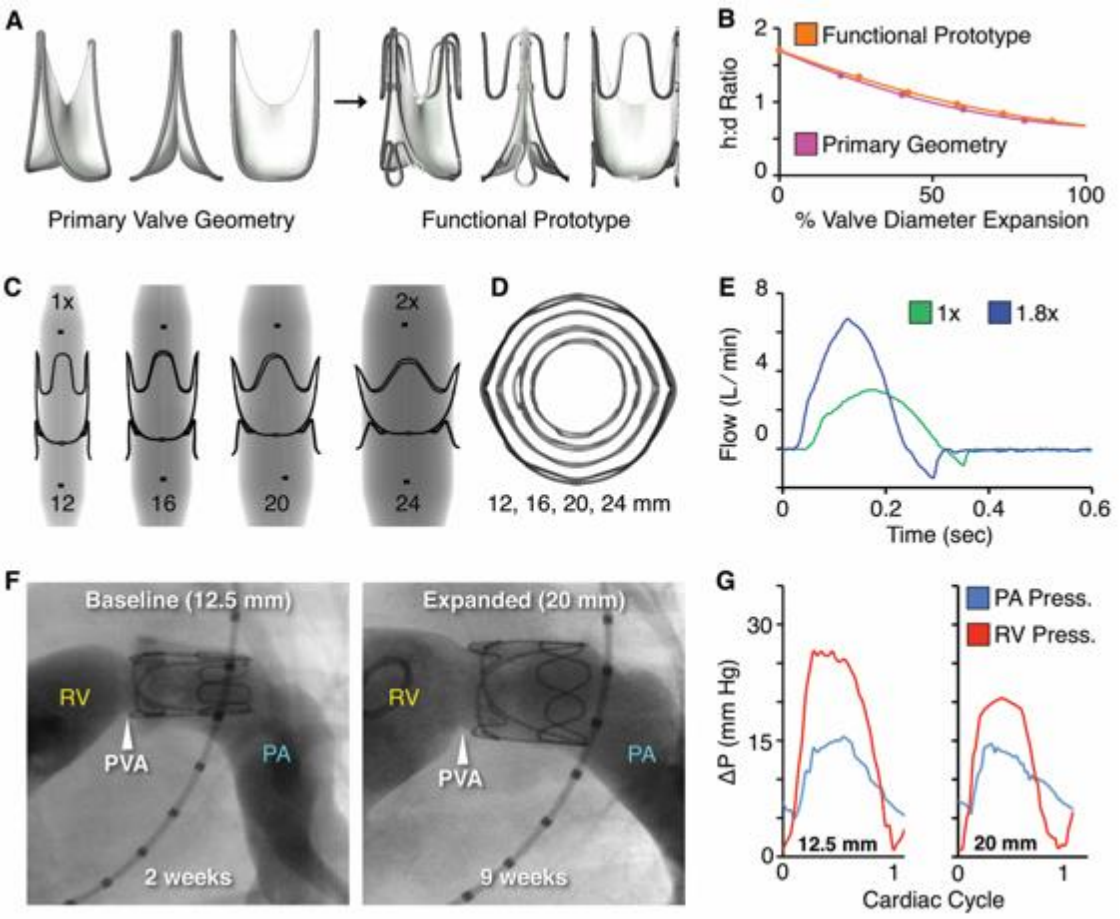

Fig. 5. Functional prototype design and *in vivo* proof-of-concept: valve expansion in a growing lamb model. (A) Structural support features added to optimize valve geometry for mechanical expansion. (**B**) Valve expansion geometry (i.e. change in aspect ratio with radial expansion) for the primary valve geometry (pink line) and functional prototype (orange line). (**C**) X-ray images of laser-cut stainless-steel functional valve prototypes being expanded via serial balloon dilation. (**D**) Top-view X-ray transmission images showing geometry of the functional prototype with expansion from 1X to 2X diameter. (**E**) *In vitro* flow loop testing of functional prototype at two polar expansion states; 1X (green) and 1.8X (blue). Plots show the valve flow cycle at both expansion states. (**F**) Representative right ventricular (RV) angiograms in a lamb showing the expandable biomimetic valve prototype in its baseline (12.5 mm ID) and

expanded (20 mm ID, post 3 separate balloon dilation procedures) configuration at 2- and 9-weeks post implantation, respectively. RV = right ventricle, PA = pulmonary artery, PVA = native pulmonary valve annulus (**G**) Representative transvalvular pressure gradient (ΔP) of the expanding biomimetic valve geometry at 2- and 9-weeks post implantation.

Necropsy and histopathological analysis demonstrated minimal tissue inflammation, a healthy right ventricle, and no evidence of distal thrombo-emboli (fig. 6). In all study animals, the pulmonary artery wall exhibited no evidence of vessel injury after chronic implantation and three transcatheter balloon expansions. There was only minimal compression of the underlying intimal and medial layers in the regions of stent contact (Fig. 6, C, D and E, S17). The ePTFE sewing cuff on the valve exterior exhibited a normal fibrocellular tissue healing response and minimal inflammatory cell infiltrate (Fig. 6. C, F, G) in all animals. The inflow and outflow surfaces of all explanted valves had minimal tissue ingrowth and were free of thrombus (blood clots). The 0.1 mm ePTFE leaflets remained intact, thin and pliable, with minimal surface irregularities and no evidence of microfractures (Figs. 6, C, F, G and H, S16, S17). There was no inflammatory cell infiltrate and no clinically significant thrombus present in any of the seven explanted valve specimens (figs. 6, S16, S17).

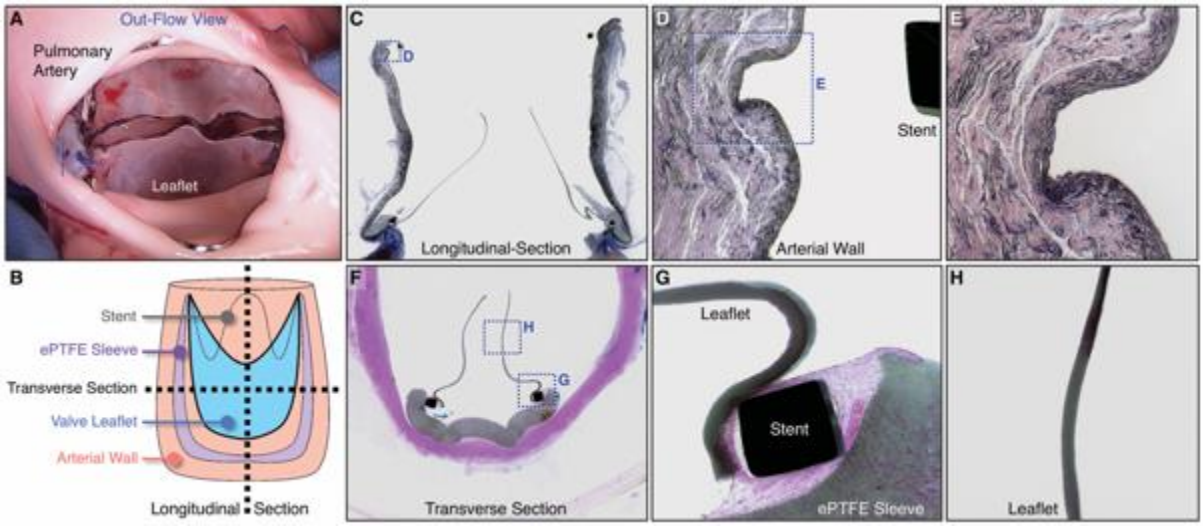

Fig. 6. ***In vivo*** **assessment of device-tissue interface: Macroscopic and histological analysis of biomimetic valve prototype implanted for 10 weeks in a growing lamb. (A)** Representative image of valve outflow surface at time of valve explant. **(B)** Schematic diagram demonstrating method of device sectioning after performing plastic embedding of the explanted specimen (valve and attached pulmonary artery). **(C)** Representative elastin stained longitudinal section of explanted valve specimen (image width = 30 mm). **(D and E)** Higher magnification images of native pulmonary artery wall, demonstrating tissue architecture at the site of vessel-stent contact and region of artery wall proximal and distal to vessel-stent interface (D, image width = 2.5 mm; E, image width = 1 mm). **(F)** Representative Hematoxylin and Eosin stained transverse section of explanted valve (image width = 20 mm). **(G)** Higher magnification image of valve leaflet at the site of stent attachment with adjacent ePTFE sleeve (image width = 2.5 mm). **(H)** Higher magnification image showing the mid-section of the valve leaflet (image width = 2.5 mm). All macroscopic and histological images shown are from the same animal.

This proof-of-concept survival study demonstrated the safety and feasibility of valve balloon expansion to accommodate somatic growth. Preserved leaflet function and the notable lack of thrombus formation, in the absence of chronic anticoagulant therapy, suggests the biomimetic

bileaflet valve geometry has favorable perivalvular flow dynamics; facilitating effective sinus washout and minimizing flow stagnation across all expansion states (See Movie S1 - term echocardiograms, color flow profile). This flow pattern appears similar to native venous valves, where flow separation and formation of large-scale vortices behind the valve leaflets prevents stasis in the sinus pockets (*39, 40*). As such, the unique fluid mechanics demonstrated in this valve design will be an important determinant of long-term device durability.

DISCUSSION

Here, we introduce a biomimetic prosthetic valve that is balloon-expandable to accommodate somatic growth and structural asymmetries within the heart, without loss of functional integrity. Benchtop and acute *in vivo* experiments validated functional performance, and *in vivo* survival studies of 9-10 weeks duration in growing lambs demonstrated successful valve balloon expansion to accommodate growth. Commercially available, non-expansile materials enabled diametric expansion without requiring redundant leaflet surface area, thus demonstrating the compatibility of this design with a variety of synthetic and tissue leaflet materials.

A growth-accommodating prosthetic heart valve would greatly advance pediatric cardiovascular medicine, since each year, over 330,000 children are born with a congenital valve defect worldwide (*1*). Moreover, acquired rheumatic heart disease affects over 5 million school-age children worldwide, many of whom require early valve replacement (*41*). Thus, existing fixed-size prostheses leaves hundreds of thousands of children to face multiple high-risk, invasive open-heart procedures over their lifetime. Moreover, valve replacement is often delayed due to size limitations of current devices, further compounding serious morbidity. Our valve design, in contrast, accommodates child growth and its adjustable dimensions enable

implantation at any age. As a result, infants and children could now potentially reach adulthood with a single valve. Such a technological breakthrough would avoid multiple surgeries, significantly reduce lifetime morbidity and mortality, and healthcare costs, as each valve replacement procedure alone costs ~$50,000 (*42*).

We envision clinical application as in our growing animal model, with valve implantation performed as soon as clinically indicated, followed by periodic valve expansion via minimally invasive transcatheter approach. Patient populations facing loss of native valve function in the first few years of life would stand to benefit tremendously from successful clinical translation of this technology. One such example is tetralogy of Fallot - the most common congenital right heart defect, accounting for ~130,000 live births per year worldwide (*1*). The serious morbidity of this defect necessitates surgical correction within the first year of life, however, current approaches fail to preserve pulmonary valve function, leading to progressive right ventricular dilation, and subsequent risk of exercise intolerance, ventricular dysfunction and life-threatening arrhythmias as these patients approach adulthood (*43-45*). To avoid these deleterious long-term outcomes, pulmonary valve replacement is performed, usually in the second decade of life. Unfortunately, though, the adverse effects of chronic valve insufficiency are often irreversible. Moreover, these children face repeated interventions to replace valves they have outgrown. Thus, a pulmonary valve replacement that is implantable during infancy and functions through to adulthood would represent a paradigm-shifting advance in the care of children with tetralogy of Fallot. We envision the timing of interventions and extent of valve expansion would be customized based on the individual child's hemodynamic and growth status.

A geometrically versatile bileaflet valve design has promise in adults as well, particularly for those where small annuli, irregular valve geometry, or intermediate valve dimensions

predispose to suboptimal procedural outcomes (*46, 47*). The ability to expand and function in non-circular, asymmetric environments may also accommodate for adults with extreme annular eccentricity (*48, 49*), native bicuspid anatomy (*50*), and those with predominant aortic regurgitation (*51*). While further work is required to enable transcatheter deployment of this device, the biomimetic size-adjustable valve design has potential to expand the indications for transcatheter valve implantation to patient subgroups currently not served by existing technology.

While we successfully demonstrated proof of concept for the expandable biomimetic valve, we acknowledge this study has limitations, and that further work is required to advance this technology towards clinical translation. First, longer-term animal studies are required to assess the chronic effects of valve implantation, including vessel remodeling, thrombosis, and leaflet degeneration/calcification in response to multiple valve dilations. Second, benchtop durability testing will be required to characterize structural integrity of the expandable biomimetic valve prototype. Third, while we used 0.1 mm ePTFE as the model leaflet material in this study, further work is required to determine if this is the optimal material for clinical applications. Thus, other substitute leaflet materials should be tested within the geometrically accommodating stent design. Fourth, stress and fatigue life analyses of the expandable stent design, including external compression testing, are necessary to identify potential failure modes and optimize frame geometry. Finally, once the optimal design is identified, we will need to explore advanced manufacturing and materials processing techniques to assemble a valve prototype for pre-clinical and, ultimately, clinical testing.

In conclusion, we demonstrate the advantage and potential of a balloon-expandable geometrically accommodating heart valve prosthesis that recapitulates the natural dimension-dynamic operation of venous valves. It is fascinating that evolution long ago optimized a valve

design for dynamic functionality. Seizing on nature, we present a bileaflet valve design of programmed dimensions and aspect ratio that adapts to growth without loss of unidirectional flow control. Controlled local fluid dynamics minimizes thrombotic, tissue hyperplastic and flow disruptions that restrict the use of current valve devices. Incorporation of these geometrically accommodating functionalities thus offers the potential for a new paradigm of care in the treatment of pediatric and adult heart valve defects.

MATERIALS AND METHODS

Study design

The objective of this study was to design a size-adjustable prosthetic heart valve that functions optimally over a wide range of dimensions. Physical prototyping using additive manufacturing techniques, finite element modeling, *in vitro* hydrodynamic performance testing, x-ray imaging, and benchtop fabrication were utilized to optimize device design. To demonstrate functional performance of the primary biomimetic valve geometry, we initially tested the device in an *in vivo*, non-survival ovine model. The device was implanted in the native pulmonary valve position of juvenile and adult sheep at two polar states of valve expansion; i) a 1X geometry (14 mm ID) valve prototype was implanted in N = 4 lambs (weight: 20 kg) and ii) a 1.8X geometry (25 mm ID) valve prototype was implanted in N = 4 adult sheep (weight: 60 kg). Animals were observed for 4-6 hours post valve implantation. Valve hemodynamic performance was assessed via continuous measurement of transvalvular pressure gradient and main pulmonary artery flow. Valve mechanical performance was evaluated via 2-D and 3-D epicardial echocardiography, performed serially during the observation period. To demonstrate proof-of-concept of our biomimetic expandable valve design, we established a preclinical *in vivo* growing lamb model. This single-arm study was not blinded or randomized. Seven lambs (aged 6 to 15 weeks) underwent surgical implantation of a 12.5 mm ID expandable biomimetic

valve prototype in the native pulmonary valve position. To accommodate somatic growth of the animal, the valve was expanded via serial transcatheter balloon dilation procedures performed at 2-, 6- and 8- weeks post-implantation. Each animal reached an expanded valve diameter of 20 mm ID (1.6X expansion). The survival period ranged from 9 to 10 weeks. Valve hemodynamic performance and heart function were investigated via serial intracardiac catheterization, angiography, and 2-D transthoracic and epicardial echocardiography. After a minimum of 63 days (range, 63 - 68 days), the valves were explanted and assessed macroscopically and histologically.

Valve prototype design and material selection

Creation, design and material selection for the venous valve-inspired bileaflet valve is described in the Supplementary Materials. Briefly, we studied the morphology and dimensions of human venous valve specimens and used these geometric design inputs to generate the biomimetic bileaflet valve geometry. To determine optimal valve length for growth accommodation, we measured the critical anatomic dimensions of the youngest pediatric patients who require heart valve replacement. We performed biaxial mechanical testing of select leaflet materials under physiologic valve loading conditions and chose a leaflet material with limited compliance to mimic the mechanical properties of native human venous valves (0.1 mm ePTFE).

Fabrication

All fabrication processes are described in detail in the Supplementary Materials. Physical prototypes of the primary biomimetic valve geometry were additively manufactured from cobalt chromium using direct metal laser sintering. Leaflets were cut from 0.1mm ePTFE (Gore® Preclude® pericardial membrane, W. L. Gore & Associates, Flagstaff, AZ, USA), and

were sewn into the leaflet attachment frame. The expandable biomimetic valve prototype was fabricated from 0.1 mm ePTFE leaflets sewn into a laser-cut stainless steel (316L) stent (Resonetics Israel Ltd, Or Akiva, Israel).

In vitro testing

In vitro hydrodynamic performance testing

Valve prototypes were tested in an *in vitro* pulsatile flow loop apparatus (ViVitro Labs Inc, Victoria, BC Canada). The *in vitro* circulatory flow loop set up is illustrated in Fig. S7. A comprehensive series of hydrodynamic experiments were performed to characterize transvalvular pressure gradient (pressure drop), effective orifice area, and valve coaptation (competence) over a wide range of physiologic and supraphysiologic flow and pressure conditions. A mixture of 0.9 ± 0.2% sodium chloride in glycerin and distilled water was used as the working fluid to emulate blood properties.

Finite Element modeling

We performed a Finite Element (FE) analysis of the biomimetic bileaflet valve. Construction and processing of the FE model is described in detail in the Supplementary Materials. Briefly, a FE model was constructed to evaluate the magnitude and distribution of stresses on the biomimetic valve leaflet in a quasi-static, closed position (diastolic phase of the cardiac cycle). The leaflet-stent model was constructed using the commercial Computer Aided Design (CAD) software SolidWorks (Dassault Systèmes, Waltham, MA, USA). The FE simulations were performed using the commercial solver ABAQUS/Explicit 2017 (Dassault Systèmes, Waltham, Mass.).

In vivo - acute ovine studies

Acute i*n vivo* studies were conducted in juvenile sheep to evaluate functional performance of the primary biomimetic valve geometry, at two polar expansion states (1X-14 mm ID, 1.8X-25 mm ID). All animal experiments were conducted in full compliance with the 1996 Guide for the Care and Use of Laboratory Animals recommended by the U.S. National Institutes of Health. The acute *in vivo* studies were performed at Boston Children's Hospital and the experimental protocol was approved by the hospital's Institutional Animal Care and Use Committee. Female Dorset lambs (N = 8, Parsons EM and Sons Inc) with a body weight of 20 kg (1X geometry, N = 4) and 60 kg (1.8X geometry, N = 4) were used. Anesthesia induction and maintenance are described in the Supplementary Materials. A left-sided thoracotomy was performed to access the chest for valve implantation and instrumentation. Transvalvular pressure gradient was evaluated via placement of right ventricular and pulmonary artery pressure lines and cardiac output was measured via perivascular flow probe (Transonics, TS420) placement around the main pulmonary artery. Epicardial echocardiographic imaging was performed to obtain native pulmonary valve and main pulmonary artery dimensions and assess overall heart function. After being heparinized (300 IU/kg), animals were cannulated for cardiopulmonary bypass. With animals cooled to 33°C and under beating heart conditions, valve prototypes were implanted in the native pulmonary valve position. Details of the surgical technique are described in the Supplementary Materials. Animals were weaned off cardiopulmonary bypass post device implantation and observed for 4 to 6 hours. 2-D epicardial echocardiography, including color and continuous wave Doppler imaging, and 3-D echocardiography were performed at multiple timepoints by a cardiologist who specializes in echocardiographic imaging. Continuous monitoring of right ventricular and pulmonary artery pressures, and main pulmonary artery flow were performed. All data were logged continuously in real time using a LabChart data logger (AD instruments). At the conclusion of the study,

animals were euthanized by intravenous injection of overdosed pentobarbital sodium (Fatal-Plus®, 86 mg/kg). The heart was excised and opened for direct inspection of the valve.

In vivo - survival ovine studies

In vivo survival studies in growing lambs were performed to demonstrate proof-of-concept of valve expansion. All survival implants were conducted at the University of Minnesota, Experimental Surgical Services animal facility. Experiments were conducted in compliance with the National Institutes of Health (NIH) Guide for the Care and Use of Laboratory Animals. The experimental protocol was approved by the University of Minnesota's Institutional Animal Care and Use Committee. Male and non-pregnant female Polypay and Hampshire breed juvenile sheep were used (N = 7, weight 22-24kg). Animal preparation, anesthesia induction and maintenance, and details of the surgical procedure are described in the Supplemental Materials. Briefly, a left thoracotomy was performed, animals were cannulated for cardiopulmonary bypass and the expandable biomimetic valve prototype was implanted in the native pulmonary valve position (See Supplementary Materials). After implantation and wean from cardiopulmonary bypass, Protamine was administered for heparin reversal. 2-D epicardial echocardiography was performed to evaluate device performance and overall heart function. Post-operatively, animals received subcutaneous Heparin (1000 IU) once the evening of surgery and then twice daily for 5 days.

To accommodate somatic growth, animals underwent transcatheter balloon dilation of the valve implant at three separate timepoints during the survival period (2-, 6-, and 8 weeks post implant). Details of the valve expansion experimental protocol are outlined in the Supplementary Materials.

Briefly, a 14Fr introducer sheath was placed in the right jugular vein. Intravenous heparin (250 mg/kg) was administered and a Swan-Ganz catheter was inserted to measure transvalvular

pressure gradient and cardiac output prior to valve dilation. Right ventricular and main pulmonary artery angiography was performed via injection of contrast and visualization under fluoroscopy. A guide wire was then introduced and an appropriately sized percutaneous balloon catheter (Atlas PTA Balloon Dilation Catheter) was advanced into position across the valve device. Under direct fluoroscopic visualization, the balloon was inflated to a nominal pressure of 6 atm to expand the valve. Valve performance and heart function were assessed post-dilation via right ventricular and main pulmonary artery angiogram and repeat measurement of transvalvular pressure gradient and cardiac output. After each valve dilation, animals received one dose of subcutaneous Heparin (1000 IU) the evening of the procedure and twice daily administration for 2 days.

Interval transthoracic echocardiography was performed to assess valve performance and heart function in the week prior to and following each scheduled balloon dilation procedure.

At term, animals were anesthetized and intracardiac hemodynamic measurements and angiographic imaging were obtained. A right thoracotomy incision exposed the heart and 2-D epicardial echocardiography was performed to assess device performance and overall heart function. Animals were euthanized by intravenous injection of phenytoin/pentobarbital solution. Necropsy was performed, with examination of the heart and valve implant. Gross pathological findings were also examined in the kidneys, lungs, brain, liver, spleen and gastrointestinal tract.

Explanted valves and attached pulmonary artery tissue were fixed in formalin and sent for plastic embedding and sectioning. Tissue samples were stained with H&E and Miller's elastic stain and examined using brightfield optical microscopy. Four representative sections were examined per animal.

Data Analysis

Hemodynamic data were analyzed using LabChart (AD Instruments). Methods of quantifying valve regurgitant volumes and transvalvular pressure gradients are described in the Supplementary Materials. Ten representative cycles for each condition were analyzed. Pulmonary artery flow, right ventricular and pulmonary artery pressures values were obtained by recording at 0.005 second intervals and then averaging the values for each over 10 consecutive cardiac cycles. Standard deviations are representative of cycle-to-cycle variations.

LIST OF SUPPLEMENTARY MATERIALS

REFERENCES AND NOTES

1. D. van der Linde, E. E. Konings, M. A. Slager, M. Witsenburg, W. A. Helbing, J. J. Takkenberg, J. W. Roos-Hesselink, Birth prevalence of congenital heart disease worldwide: a systematic review and meta-analysis. *J Am Coll Cardiol* **58**, 2241-2247 (2011).
2. P. L. Bernier, A. Stefanescu, G. Samoukovic, C. I. Tchervenkov, The challenge of congenital heart disease worldwide: epidemiologic and demographic facts. *Semin Thorac Cardiovasc Surg Pediatr Card Surg Annu* **13**, 26-34 (2010).
3. S. M. Gilboa, O. J. Devine, J. E. Kucik, M. E. Oster, T. Riehle-Colarusso, W. N. Nembhard, P. Xu, A. Correa, K. Jenkins, A. J. Marelli, Congenital Heart Defects in the United States: Estimating the Magnitude of the Affected Population in 2010. *Circulation* **134**, 101-109 (2016).
4. E. J. Benjamin, M. J. Blaha, S. E. Chiuve, M. Cushman, S. R. Das, R. Deo, S. D. de Ferranti, J. Floyd, M. Fornage, C. Gillespie, C. R. Isasi, M. C. Jimenez, L. C. Jordan, S. E. Judd, D. Lackland, J. H. Lichtman, L. Lisabeth, S. Liu, C. T. Longenecker, R. H. Mackey, K. Matsushita, D. Mozaffarian, M. E. Mussolino, K. Nasir, R. W. Neumar, L. Palaniappan, D. K. Pandey, R. R. Thiagarajan, M. J. Reeves, M. Ritchey, C. J. Rodriguez, G. A. Roth, W. D. Rosamond, C. Sasson, A. Towfighi, C. W. Tsao, M. B. Turner, S. S. Virani, J. H. Voeks, J. Z. Willey, J. T. Wilkins, J. H. Wu, H. M. Alger, S. S. Wong, P. Muntner, C. American Heart Association Statistics, S. Stroke Statistics, Heart Disease and Stroke Statistics-2017 Update: A Report From the American Heart Association. *Circulation* **135**, e146-e603 (2017).
5. J. Hoffman, The global burden of congenital heart disease. *Cardiovasc J Afr* **24**, 141-145 (2013).

6. S. A. Husain, J. W. Brown, When reconstruction fails or is not feasible: valve replacement options in the pediatric population. *Semin Thorac Cardiovasc Surg Pediatr Card Surg Annu*, 117-124 (2007).

7. P. C. Chen, M. S. Sager, D. Zurakowski, F. A. Pigula, C. W. Baird, J. E. Mayer, Jr., P. J. Del Nido, S. M. Emani, Younger age and valve oversizing are predictors of structural valve deterioration after pulmonary valve replacement in patients with tetralogy of Fallot. *J Thorac Cardiovasc Surg* **143**, 352-360 (2012).

8. T. Karamlou, E. H. Blackstone, J. A. Hawkins, M. L. Jacobs, K. R. Kanter, J. W. Brown, C. Mavroudis, C. A. Caldarone, W. G. Williams, B. W. McCrindle, S. Pulmonary Conduit Working Group for the members of the Congenital Heart Surgeons, Can pulmonary conduit dysfunction and failure be reduced in infants and children less than age 2 years at initial implantation? *J Thorac Cardiovasc Surg* **132**, 829-838 (2006).

9. B. Lubiszewska, J. Rozanski, M. Szufladowicz, W. Szaroszyk, P. Hoffman, E. Ksiezycka, W. Rydlewska-Sadowska, W. Ruzyllo, Mechanical valve replacement in congenital heart disease in children. *J Heart Valve Dis* **8**, 74-79 (1999).

10. R. Henaine, F. Roubertie, M. Vergnat, J. Ninet, Valve replacement in children: a challenge for a whole life. *Arch Cardiovasc Dis* **105**, 517-528 (2012).

11. B. Alsoufi, C. Manlhiot, M. Al-Ahmadi, B. W. McCrindle, A. Kalloghlian, G. Siblini, Z. Bulbul, Z. Al-Halees, Outcomes and associated risk factors for mitral valve replacement in children. *Eur J Cardiothorac Surg* **40**, 543-551 (2011).

12. T. Karamlou, K. Jang, W. G. Williams, C. A. Caldarone, G. Van Arsdell, J. G. Coles, B. W. McCrindle, Outcomes and associated risk factors for aortic valve replacement in 160 children: a competing-risks analysis. *Circulation* **112**, 3462-3469 (2005).

13. R. Nomoto, L. A. Sleeper, M. J. Borisuk, L. Bergerson, F. A. Pigula, S. Emani, F. Fynn-Thompson, J. E. Mayer, P. J. Del Nido, C. W. Baird, Outcome and performance of bioprosthetic pulmonary valve replacement in patients with congenital heart disease. *J Thorac Cardiovasc Surg* **152**, 1333-1342 e1333 (2016).

14. K. R. Kanter, J. M. Forbess, P. M. Kirshbom, Redo mitral valve replacement in children. *Ann Thorac Surg* **80**, 642-645; discussion 645-646 (2005).

15. K. R. Kanter, P. M. Kirshbom, B. E. Kogon, Redo aortic valve replacement in children. *Ann Thorac Surg* **82**, 1594-1597 (2006).

16. R. K. Woods, S. K. Pasquali, M. L. Jacobs, E. H. Austin, J. P. Jacobs, M. Krolikowski, M. E. Mitchell, C. Pizarro, J. S. Tweddell, Aortic valve replacement in neonates and infants: an analysis of the Society of Thoracic Surgeons Congenital Heart Surgery Database. *J Thorac Cardiovasc Surg* **144**, 1084-1089 (2012).

17. N. Faza, D. Kenny, C. Kavinsky, Z. Amin, M. Heitschmidt, Z. M. Hijazi, Single-center comparative outcomes of the Edwards SAPIEN and Medtronic Melody transcatheter heart valves in the pulmonary position. *Catheter Cardiovasc Interv* **82**, E535-541 (2013).

18. D. B. McElhinney, W. E. Hellenbrand, E. M. Zahn, T. K. Jones, J. P. Cheatham, J. E. Lock, J. A. Vincent, Short- and medium-term outcomes after transcatheter pulmonary valve placement in the expanded multicenter US melody valve trial. *Circulation* **122**, 507-516 (2010).

19. D. P. Berman, D. B. McElhinney, J. A. Vincent, W. E. Hellenbrand, E. M. Zahn, Feasibility and short-term outcomes of percutaneous transcatheter pulmonary valve replacement in small (<30 kg) children with dysfunctional right ventricular outflow tract conduits. *Circ Cardiovasc Interv* **7**, 142-148 (2014).

20. S. Schievano, L. Coats, F. Migliavacca, W. Norman, A. Frigiola, J. Deanfield, P. Bonhoeffer, A. M. Taylor, Variations in right ventricular outflow tract morphology following repair of congenital heart disease: implications for percutaneous pulmonary valve implantation. *J Cardiovasc Magn Reson* **9**, 687-695 (2007).

21. L. M. de Heer, R. P. Budde, W. P. Mali, A. M. de Vos, L. A. van Herwerden, J. Kluin, Aortic root dimension changes during systole and diastole: evaluation with ECG-gated multidetector row computed tomography. *Int J Cardiovasc Imaging* **27**, 1195-1204 (2011).

22. T. Kazui, H. Izumoto, K. Yoshioka, K. Kawazoe, Dynamic morphologic changes in the normal aortic annulus during systole and diastole. *J Heart Valve Dis* **15**, 617-621 (2006).

23. M. Cantinotti, R. Giordano, M. Scalese, B. Murzi, N. Assanta, I. Spadoni, C. Maura, M. Marco, S. Molinaro, S. Kutty, G. Iervasi, Nomograms for two-dimensional echocardiography derived valvular and arterial dimensions in Caucasian children. *J Cardiol* **69**, 208-215 (2017).

24. P. E. Hammer, E. G. Roberts, S. M. Emani, P. J. Del Nido, Surgical reconstruction of semilunar valves in the growing child: Should we mimic the venous valve? A simulation study. *J Thorac Cardiovasc Surg* **153**, 389-396 (2017).

25. P. Pibarot, J. G. Dumesnil, Prosthetic heart valves: selection of the optimal prosthesis and long-term management. *Circulation* **119**, 1034-1048 (2009).

26. J. Sathananthan, S. Sellers, A. Barlow, R. Fraser, V. Stanova, A. Cheung, J. Ye, A. Alenezi, D. J. Murdoch, M. Hensey, D. Dvir, P. Blanke, R. Rieu, D. Wood, P. Pibarot, J. Leipsic, J. Webb, Overexpansion of the SAPIEN 3 Transcatheter Heart Valve: An Ex Vivo Bench Study. *JACC Cardiovasc Interv* **11**, 1696-1705 (2018).

27. C. F. Rothe, Reflex control of veins and vascular capacitance. *Physiol Rev* **63**, 1281-1342 (1983).

28. R. Hainsworth, Vascular capacitance: its control and importance. *Rev Physiol Biochem Pharmacol* **105**, 101-173 (1986).

29. F. Lurie, R. L. Kistner, B. Eklof, The mechanism of venous valve closure in normal physiologic conditions. *J Vasc Surg* **35**, 713-717 (2002).

30. M. G. Vancov G, Construction of the Microcirculatory vascular bed in the venous wall. *Acta Morph Bulg Acad Sci* **5**, 20-23 (1984).

31. K. J. Franklin, Valves in Veins: An Historical Survey. *Proc R Soc Med* **21**, 1-33 (1927).

32. E. A. Edwards, The Treatment of varicose veins; anatomical factors of ligation of the great saphenous vein. *Surgery, Gynecology & Obstetrics* **59**, 916-928 (1934).

33. G. L. Moneta, G. Bedford, K. Beach, D. E. Strandness, Duplex ultrasound assessment of venous diameters, peak velocities, and flow patterns. *J Vasc Surg* **8**, 286-291 (1988).

34. T. Miyazaki, M. Yamagishi, Y. Maeda, S. Taniguchi, S. Fujita, H. Hongu, H. Yaku, Long-term outcomes of expanded polytetrafluoroethylene conduits with bulging sinuses and a fan-shaped valve in right ventricular outflow tract reconstruction. *J Thorac Cardiovasc Surg* **155**, 2567-2576 (2018).

35. C. Martin, W. Sun, Simulation of long-term fatigue damage in bioprosthetic heart valves: effects of leaflet and stent elastic properties. *Biomech Model Mechanobiol* **13**, 759-770 (2014).

36. W. Sun, A. Abad, M. S. Sacks, Simulated bioprosthetic heart valve deformation under quasi-static loading. *J Biomech Eng* **127**, 905-914 (2005); published online EpubNov (

37. I. Vesely, The evolution of bioprosthetic heart valve design and its impact on durability. *Cardiovasc Pathol* **12**, 277-286 (2003).

38. Y. Xuan, K. Krishnan, J. Ye, D. Dvir, J. M. Guccione, L. Ge, E. E. Tseng, Stent and leaflet stresses in a 26-mm first-generation balloon-expandable transcatheter aortic valve. *J Thorac Cardiovasc Surg* **153**, 1065-1073 (2017).

39. F. Lurie, R. L. Kistner, B. Eklof, D. Kessler, Mechanism of venous valve closure and role of the valve in circulation: a new concept. *J Vasc Surg* **38**, 955-961 (2003).

40. K. H. Nam, E. Yeom, H. Ha, S. J. Lee, Velocity field measurements of valvular blood flow in a human superficial vein using high-frequency ultrasound speckle image velocimetry. *Int J Cardiovasc Imaging* **28**, 69-77 (2012).

41. K. B. Tibazarwa, J. A. Volmink, B. M. Mayosi, Incidence of acute rheumatic fever in the world: a systematic review of population-based studies. *Heart* **94**, 1534-1540 (2008).

42. M. L. O'Byrne, M. J. Gillespie, R. T. Shinohara, Y. Dori, J. J. Rome, A. C. Glatz, Cost comparison of Transcatheter and Operative Pulmonary Valve Replacement (from the Pediatric Health Information Systems Database). *Am J Cardiol* **117**, 121-126 (2016).

43. T. Geva, Indications and timing of pulmonary valve replacement after tetralogy of Fallot repair. *Semin Thorac Cardiovasc Surg Pediatr Card Surg Annu*, 11-22 (2006).

44. J. G. Murphy, B. J. Gersh, D. D. Mair, V. Fuster, M. D. McGoon, D. M. Ilstrup, D. C. McGoon, J. W. Kirklin, G. K. Danielson, Long-term outcome in patients undergoing surgical repair of tetralogy of Fallot. *N Engl J Med* **329**, 593-599 (1993).

45. G. Nollert, T. Fischlein, S. Bouterwek, C. Bohmer, W. Klinner, B. Reichart, Long-term survival in patients with repair of tetralogy of Fallot: 36-year follow-up of 490 survivors of the first year after surgical repair. *J Am Coll Cardiol* **30**, 1374-1383 (1997).

46. L. Buellesfeld, S. Stortecky, D. Heg, S. Gloekler, B. Meier, P. Wenaweser, S. Windecker, Extent and distribution of calcification of both the aortic annulus and the

left ventricular outflow tract predict aortic regurgitation after transcatheter aortic valve replacement. *EuroIntervention* **10**, 732-738 (2014).

47. M. Nakashima, Y. Watanabe, Transcatheter Aortic Valve Implantation in Small Anatomy: Patient Selection and Technical Challenges. *Interv Cardiol* **13**, 66-68 (2018).

48. M. Barbanti, T. H. Yang, J. Rodes Cabau, C. Tamburino, D. A. Wood, H. Jilaihawi, P. Blanke, R. R. Makkar, A. Latib, A. Colombo, G. Tarantini, R. Raju, R. K. Binder, G. Nguyen, M. Freeman, H. B. Ribeiro, S. Kapadia, J. Min, G. Feuchtner, R. Gurtvich, F. Alqoofi, M. Pelletier, G. P. Ussia, M. Napodano, F. S. de Brito, Jr., S. Kodali, B. L. Norgaard, N. C. Hansson, G. Pache, S. J. Canovas, H. Zhang, M. B. Leon, J. G. Webb, J. Leipsic, Anatomical and procedural features associated with aortic root rupture during balloon-expandable transcatheter aortic valve replacement. *Circulation* **128**, 244-253 (2013).

49. A. Masri, P. Schoenhagen, L. Svensson, S. R. Kapadia, B. P. Griffin, E. M. Tuzcu, M. Y. Desai, Dynamic characterization of aortic annulus geometry and morphology with multimodality imaging: predictive value for aortic regurgitation after transcatheter aortic valve replacement. *J Thorac Cardiovasc Surg* **147**, 1847-1854 (2014).

50. S. H. Yoon, S. Bleiziffer, O. De Backer, V. Delgado, T. Arai, J. Ziegelmueller, M. Barbanti, R. Sharma, G. Y. Perlman, O. K. Khalique, E. W. Holy, S. Saraf, F. Deuschl, B. Fujita, P. Ruile, F. J. Neumann, G. Pache, M. Takahashi, H. Kaneko, T. Schmidt, Y. Ohno, N. Schofer, W. K. F. Kong, E. Tay, D. Sugiyama, H. Kawamori, Y. Maeno, Y. Abramowitz, T. Chakravarty, M. Nakamura, S. Kuwata, G. Yong, H. L. Kao, M. Lee, H. S. Kim, T. Modine, S. C. Wong, F. Bedgoni, L. Testa, E. Teiger, C. Butter, S. M. Ensminger, U. Schaefer, D. Dvir, P. Blanke, J. Leipsic, F. Nietlispach, M. Abdel-Wahab, B. Chevalier, C. Tamburino, D. Hildick-Smith, B. K. Whisenant, S. J. Park, A. Colombo, A. Latib, S. K. Kodali, J. J. Bax, L. Sondergaard, J. G. Webb, T. Lefevre, M.

B. Leon, R. Makkar, Outcomes in Transcatheter Aortic Valve Replacement for Bicuspid Versus Tricuspid Aortic Valve Stenosis. *J Am Coll Cardiol* **69**, 2579-2589 (2017).

51. S. H. Yoon, T. Schmidt, S. Bleiziffer, N. Schofer, C. Fiorina, A. J. Munoz-Garcia, E. Yzeiraj, I. J. Amat-Santos, D. Tchetche, C. Jung, B. Fujita, A. Mangieri, M. A. Deutsch, T. Ubben, F. Deuschl, S. Kuwata, C. De Biase, T. Williams, A. Dhoble, W. K. Kim, E. Ferrari, M. Barbanti, E. M. Vollema, A. Miceli, C. Giannini, G. F. Attizzani, W. K. F. Kong, E. Gutierrez-Ibanes, V. A. Jimenez Diaz, H. C. Wijeysundera, H. Kaneko, T. Chakravarty, M. Makar, H. Sievert, C. Hengstenberg, B. D. Prendergast, F. Vincent, M. Abdel-Wahab, L. Nombela-Franco, M. Silaschi, G. Tarantini, C. Butter, S. M. Ensminger, D. Hildick-Smith, A. S. Petronio, W. H. Yin, F. De Marco, L. Testa, N. M. Van Mieghem, B. K. Whisenant, K. H. Kuck, A. Colombo, S. Kar, C. Moris, V. Delgado, F. Maisano, F. Nietlispach, M. J. Mack, J. Schofer, U. Schaefer, J. J. Bax, C. Frerker, A. Latib, R. R. Makkar, Transcatheter Aortic Valve Replacement in Pure Native Aortic Valve Regurgitation. *J Am Coll Cardiol* **70**, 2752-2763 (2017).

52. W. A. Helbing, H. G. Bosch, C. Maliepaard, S. A. Rebergen, R. J. van der Geest, B. Hansen, J. Ottenkamp, J. H. Reiber, A. de Roos, Comparison of echocardiographic methods with magnetic resonance imaging for assessment of right ventricular function in children. *Am J Cardiol* **76**, 589-594 (1995).

53. R. M. Lang, M. Bierig, R. B. Devereux, F. A. Flachskampf, E. Foster, P. A. Pellikka, M. H. Picard, M. J. Roman, J. Seward, J. S. Shanewise, S. D. Solomon, K. T. Spencer, M. S. Sutton, W. J. Stewart, G. Chamber Quantification Writing, G. American Society of Echocardiography's, C. Standards, E. European Association of, Recommendations for chamber quantification: a report from the American Society of Echocardiography's Guidelines and Standards Committee and the Chamber Quantification Writing Group,

developed in conjunction with the European Association of Echocardiography, a branch of the European Society of Cardiology. *J Am Soc Echocardiogr* **18**, 1440-1463 (2005).

54. L. Lopez, S. D. Colan, P. C. Frommelt, G. J. Ensing, K. Kendall, A. K. Younoszai, W. W. Lai, T. Geva, Recommendations for quantification methods during the performance of a pediatric echocardiogram: a report from the Pediatric Measurements Writing Group of the American Society of Echocardiography Pediatric and Congenital Heart Disease Council. *J Am Soc Echocardiogr* **23**, 465-495; quiz 576-467 (2010).
55. S. C. Hofferberth, C. W. Baird, D. M. Hoganson, L. G. Quinonez, S. M. Emani, P. J. Del Nido, P. E. Hammer, Mechanical Properties of Autologous Pericardium Change With Fixation Time: Implications for Valve Reconstruction. *Semin Thorac Cardiovasc Surg*, (2019).
56. S. B. Capps, R. C. Elkins, D. M. Fronk, Body surface area as a predictor of aortic and pulmonary valve diameter. *J Thorac Cardiovasc Surg* **119**, 975-982 (2000).

ACKNOWLEDGEMENTS

We thank Richard M. Bianco, John Carney and the Experimental Surgical Services lab for help with design of the survival animal studies and for conducting the experiments, John E. Mayer for surgical expertise and helpful discussions, Christopher W. Baird for helpful discussions, Oliver Barry and Brian Quinn for technical support with animal procedures. **Funding:** S.C.H was supported by a National Institutes of Health - NRSA post-doctoral fellowship grant (1F32HL138993-01) and an Early Career Award from the Thrasher Research Fund. **Author contributions:** S.C.H developed the concept, designed the valve and performed the experiments, analyzed the data, and wrote the manuscript. M.S contributed to performance of

animal experiments, L.T generated the anatomical models and animations and contributed to manuscript preparation, M.F developed computational models for data analysis and contributed to manuscript preparation, C.P contributed to valve design and CAD modeling, K.P contributed to CAD modeling and experimental design, G.R.M, J.J.E, D.W.B contributed to data analysis and performance of animal experiments, J.B contributed to the design of *in vitro* experiments, P.E.H contributed to experimental design and data analysis, J.C.W coordinated 3D anatomical modeling and FEA studies and contributed to manuscript preparation. E.R.E contributed to experimental design, data analysis, manuscript preparation and study oversight. P.J.d.N contributed to project conception, experimental design, data analysis, manuscript preparation and supervised the overall project. All authors read and edited the final version of the manuscript. **Competing Interests:** S.C.H, P.J.d.N, E.R.E, P.E.H, C.P have a provisional patent application entitled "Geometrically-accommodating heart valve replacement device" (WO2019099864). **Data and materials availability:** Data are available in the supplementary materials.

Supplementary Materials for

A geometrically accommodating heart valve replacement

Sophie C. Hofferberth*, Mossab Y. Saeed, Lara Tomholt, Matheus C. Fernandes, Christopher Payne, Karl Price, Gerald R. Marx, Jesse J. Esch, David W. Brown, Jonathan Brown, Peter E. Hammer, James C. Weaver, Elazer R. Edelman, Pedro J. del Nido*

*Correspondence to:

Sophie C. Hofferberth: sophie.hofferberth@cardio.chboston.org

Pedro J. del Nido: pedro.delnido@cardio.chboston.org

This file includes:

Characterization of venous valve geometry

To create the venous valve-inspired leaflet geometry, we studied the morphology of native human venous valves, obtained from commercial sources. We took measurements from cryopreserved human femoral (N = 1) and saphenous vein (N = 1) grafts (CryoLife Inc., Kennesaw, GA) (fig. S1A). The native diameter of the femoral and saphenous vein specimens was 8 mm and 3 mm, respectively. Each vein graft specimen contained multiple valves (femoral vein, N = 2; saphenous vein, N = 2).

The cryopreserved vein grafts were initially thawed in a warm water bath. Specimens were then incised longitudinally, and the location of each valve was confirmed (fig. S1B). Valve dimensions were measured in the non-distended state (fig. S1C). Valve height, defined as the linear distance from the top of the valve commissure (where leaflets meet and insert into the vessel wall) to the base of the leaflet, valve diameter, and leaflet mid-height (linear distance from top of valve commissure to nadir of leaflet free edge) were measured for each venous valve (N = 4) (fig. S1C). Mean values were calculated for each dimension across all specimens. The geometry of the 3-dimensional leaflet-vessel wall attachment curve was also recorded for each valve specimen (fig. S1C).

Mean valve height to diameter ratio was 2.03:1 ± 0.06 and mean leaflet mid-height to commissural height ratio was 0.495:1 ± 0.02. The morphology and dimensions of the native venous valve specimens were used to design the leaflet geometry of the biomimetic primary valve prototype (fig. S1D).

Table S1. Native human venous valve measurements

Human Venous valve specimen	Valve height (mm)	Valve diameter (mm)	Valve height: diameter ratio	Leaflet mid-height (mm)	Leaflet mid-height: overall height ratio
1	16	8	2:1	8	0.5:1
2	17	8	2.125:1	8	0.47:1
3	6	3	2:1	3	0.5:1
4	6	3	2:1	3	0.5:1

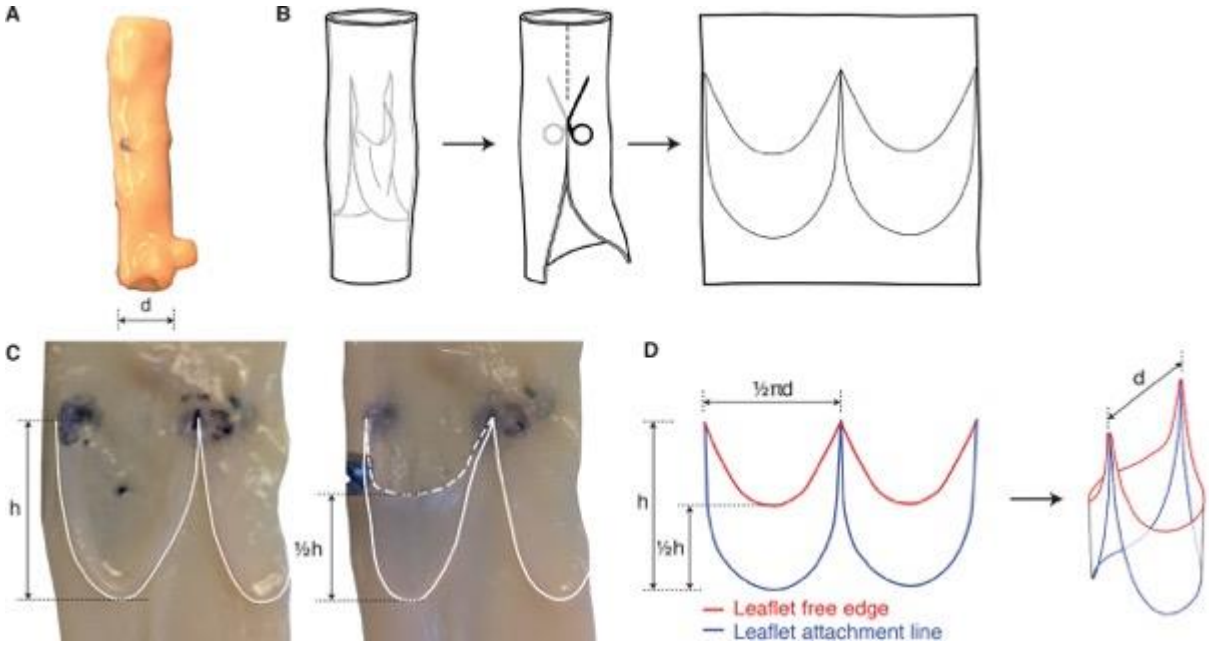

Fig. S1: Determination of human venous valve geometry and dimensions. (a) human saphenous vein specimen, **(b)** method of vein dissection to expose venous valve, **(c)** unrolled human venous valve specimen with outline of leaflet-vessel wall attachment and leaflet free edge (dotted line), and **(d)** key dimensions and geometric features of human venous valve used to inform biomimetic valve design.

Generation of biomimetic bileaflet valve geometry

The three key geometric features of the biomimetic valve design are 1) the leaflet profile geometry, 2) the 3-dimensional leaflet attachment geometry, and 3) the valve expansion geometry. We developed methods for geometrically describing these features based on two parameters: the valve height (H) and the valve diameter (D). Digitized geometry was generated in a solid modeling computer aided design (CAD) software SolidWorks (Dassault Systèmes, Waltham, MA, USA).

Leaflet profile geometry

The leaflet profile geometry was defined as a 2D geometric profile that was created based on the morphology and dimensions observed in human venous valve specimens (fig. S1). For a given valve, the leaflet profile was scaled such that the commissure-to-commissure length is defined as half the valve circumference ($0.5\pi D$) and the commissure-to-base length is equivalent to the valve height (H). The leaflet mid-height (L_H) was defined as 0.5H in accordance with human venous valve dimensions (fig. S2A).

Leaflet attachment geometry

We defined the leaflet attachment geometry as the geometric profile created by the native venous valve leaflet joining to the surrounding vessel wall. This attachment geometry can be approximated as a three-dimensional (3D) curve. To obtain this curve profile, we projected an elliptical quadrant onto a cylinder, which represents the inner wall of a vessel (fig. S2B). The ellipse profile had a semi-major axis length equivalent to the height of the valve (H) and a semi-minor axis with a length equivalent to the radius (r) of the valve. The cylinder had a radius equivalent to that of the valve. The ellipse was then normally projected onto the cylinder; the ellipse co-vertex was made to be coincident with the cylinder centerline and the ellipse vertices and center were all coincident with the outer edge of the cylinder when viewed from the side projection (fig. S2B). The resulting 3D curve projections were mirrored about the centerline of the cylinder to generate the attachment geometry for the second leaflet.

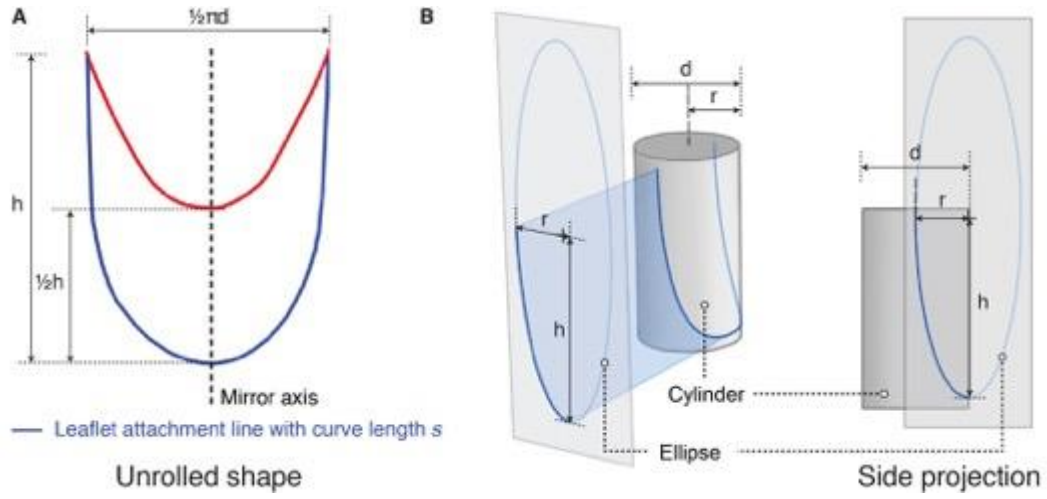

Fig S2: Methodology for creating biomimetic primary valve geometry (A) leaflet profile geometry. **(B)** Geometrical projection of elliptical quadrant on to cylinder to create 3-dimensional leaflet attachment geometry

Expanding valve geometry

We developed a methodology for diametrically expanding the valve leaflet attachment geometry to approximate radial expansion of a growing artery/valve annulus. We fixed the perimeter length of the 3-dimensional leaflet attachment curve (s) so that radial expansion was accompanied by a reduction in valve height (Fig S3A). The varying aspect ratio leaflet attachment geometry is a critical feature of our biomimetic valve design. We firstly defined a baseline leaflet attachment geometry for a baseline height (HB) and a baseline diameter (DB). Next, we computed the curve length of the baseline leaflet attachment curve (s). We then generated expanded valve geometries by computing the valve height (H) from the expanded diameter (D) and fixed length of the leaflet attachment curve (s). Fig. S3B shows the decreasing height-to-diameter ratio (H/D) for an expanding valve from initial diameter DB to the largest expansion diameter at which a given valve geometry stays functional. The plots represent valve geometries with various baseline HB/DB ratios, including 2, 1.7 and 1.5.

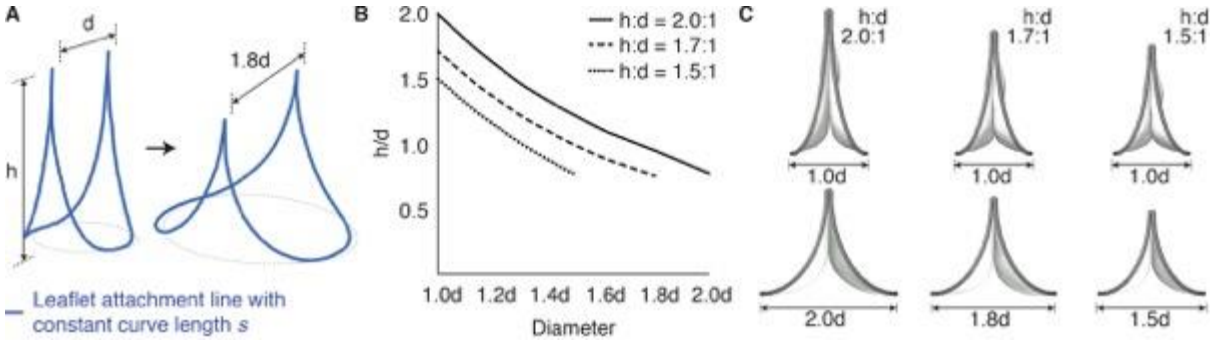

Fig S3: Expanding valve geometry. (A) Methodology for expanding leaflet attachment geometry of initial height-to-diameter ratio by constraining perimeter length. **(B)** height-to-diameter ratio change as a function of fixed length leaflet attachment geometry diameter. (**C**) Baseline aspect ratio determines extent of functional valve expansion.

Optimal valve height-to-diameter ratio for pediatric patients

Our goal was to design a size-adjustable prosthetic heart valve with dimensions suitable for implantation from infancy through to adulthood. To determine these design parameters, we investigated the critical anatomic dimensions of the youngest pediatric patients who require heart valve replacement. Tetralogy of Fallot (ToF) is the most common congenital right heart defect and accounts for nearly 10% of all children born with heart anomalies (*1*). The native pulmonary valve in ToF is usually abnormal and prohibits normal outflow of blood to the lungs. The serious morbidity of this defect necessitates surgical correction in the first few months of life, however current approaches fail to preserve pulmonary valve function. Thus, our valve dimensions (i.e. height and diameter) needed to be suitable for implantation in ToF patients undergoing surgical repair in early infancy.

Since the native pulmonary valve annulus diameter is generally severely hypoplastic (undersized) in ToF patients, we referenced population-based echocardiographic data to determine the optimum baseline valve diameter. These data indicate that a normal sized pulmonary valve annulus diameter is approximately 10 mm in a 3-month-old child (*23*), which we used as the baseline valve internal diameter for subsequent investigations.

To determine the optimum valve height: diameter ratio, we measured the length of the main pulmonary artery in a cohort of ToF patients who underwent surgical repair at Boston Children's Hospital. Institutional Review Board approval was obtained, and a waiver of documented patient consent was granted. We performed a retrospective echocardiographic analysis in 22 patients, aged less than 6 months, who underwent primary repair of ToF at Boston Children's Hospital between August 2014 and August 2016.

Imaging of the right ventricular outflow tract and pulmonary artery was performed using standard echocardiographic views (*52-54*) (fig. S4A). A single reviewer independently obtained measurements from the pre-operative 2-dimensional (2D) transthoracic echocardiogram (TTE) in all patients. A second independent and blinded reviewer measured a

random sample. All echocardiographic measurements were analyzed using Image-Arena software (versions 4.6; Tom-Tec Imaging Systems, Unterschleissheim, Germany). Main pulmonary artery length was defined as the linear distance between the pulmonary valve annulus and the bifurcation (branch point) of the left and right pulmonary arteries (fig. S4B), and the anatomic location of the pulmonary artery bifurcation was confirmed by color flow imaging in the same view (fig. S4C). The measurement was performed 3 times in each patient and the mean value was recorded. Among the 22 patients, mean age was 89.6 ± 29 days and mean length of the main pulmonary artery was 17.9 ± 2.8 mm.

Based on this data, the maximum acceptable prosthesis height is 17 mm for this particular population of infant patients. Thus, given a baseline valve diameter of 10 mm, we determined a suitable valve aspect ratio for pediatric patients is 1.7:1.

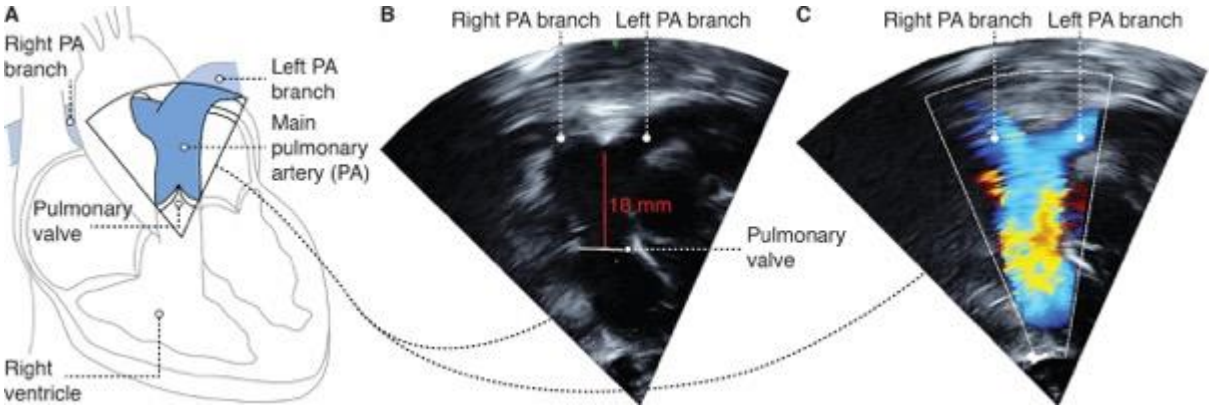

Fig S4: Determination of optimal valve dimensions for pediatric patients: echocardiographic imaging of infants with tetralogy of Fallot. (A) Illustration showing echocardiographic view of an infant heart, **(B)** representative 2-D echocardiographic image illustrating the pulmonary artery dimensions, and **(C)** corresponding 2-D echocardiographic image with color flow doppler.

Leaflet material selection and characterization

We sought a leaflet material with limited compliance (inextensible) to mimic mechanical properties of the native venous valve leaflet and test our hypothesis that a varying aspect ratio valve design enables radial expansion without necessitating an increase in leaflet surface area. We therefore chose 0.1 mm thickness expanded polytetrafluoroethylene (ePTFE) (Goretex® Preclude® pericardial membrane, W. L. Gore & Associates, Flagstaff, AZ USA) as the model leaflet material for our biomimetic valve prototype. This material was chosen as ePTFE is biocompatible, relatively inextensible, and is currently used for intra-cardiac procedures. We performed biaxial mechanical testing to quantify material extensibility and anisotropy.

A 5-N capacity biaxial testing device (Biotester, CellScale, Waterloo, Canada) was used to perform mechanical testing of the 0.1 mm ePTFE Goretex material (fig. S5A, B).

Identification of material orientation

To identify principal material orientation, a square section of material was cut from a 15 cm x 20 cm sheet of commercial 0.1 mm thickness ePTFE. The employed mechanical testing protocol was the same as previously described by our group (*55*) and outlined below.

Samples were cut into 10 mm x 10 mm squares (fig. S5C), and material thickness was confirmed in 3 regions across each sample using an electronic thickness gauge (Model CD-68CT, Mitutoyo, Japan). Samples were affixed to four tungsten rakes, and each rake was fitted with 5 tines spaced at 1.0 mm (fig. S5C). The resulting test specimens were then immersed in a temperature-controlled (37 °C) bath to emulate *in vivo* conditions.

Experimental protocol

A biaxial testing protocol was developed using the Biotester equipment software (LabJoy). The LabJoy data acquisition module was utilized to set 1) the parameters for the test phase of each load cycle, 2) the water bath temperature, and 3) the data and image acquisition rate (15 Hz). The test protocol involved application of preload to samples, stretch, hold, recovery, and rest. Biaxial testing was performed with the Biotester system in force-control mode (fig. S5D).

To approximate physiologic valve loading conditions, we tested samples at a maximal loading condition of 1 N, and each sample was subjected to preconditioning cycles prior to evaluation. Samples were initially subjected to 10 cycles of equibiaxial stretch at 1 N, followed by seven proportional biaxial cycles at load ratios (Y:X) of 0.25:1, 0.5:1.0, 0.75:1.0, 1.0:1.0, 1.0:0.75, 1.0:0.5, 1.0:0.25 N (fig. S5D).

Computation of stresses and strains

The strain field across samples was estimated using a combination of the Labjoy software and customized software, as previously described (*56*).

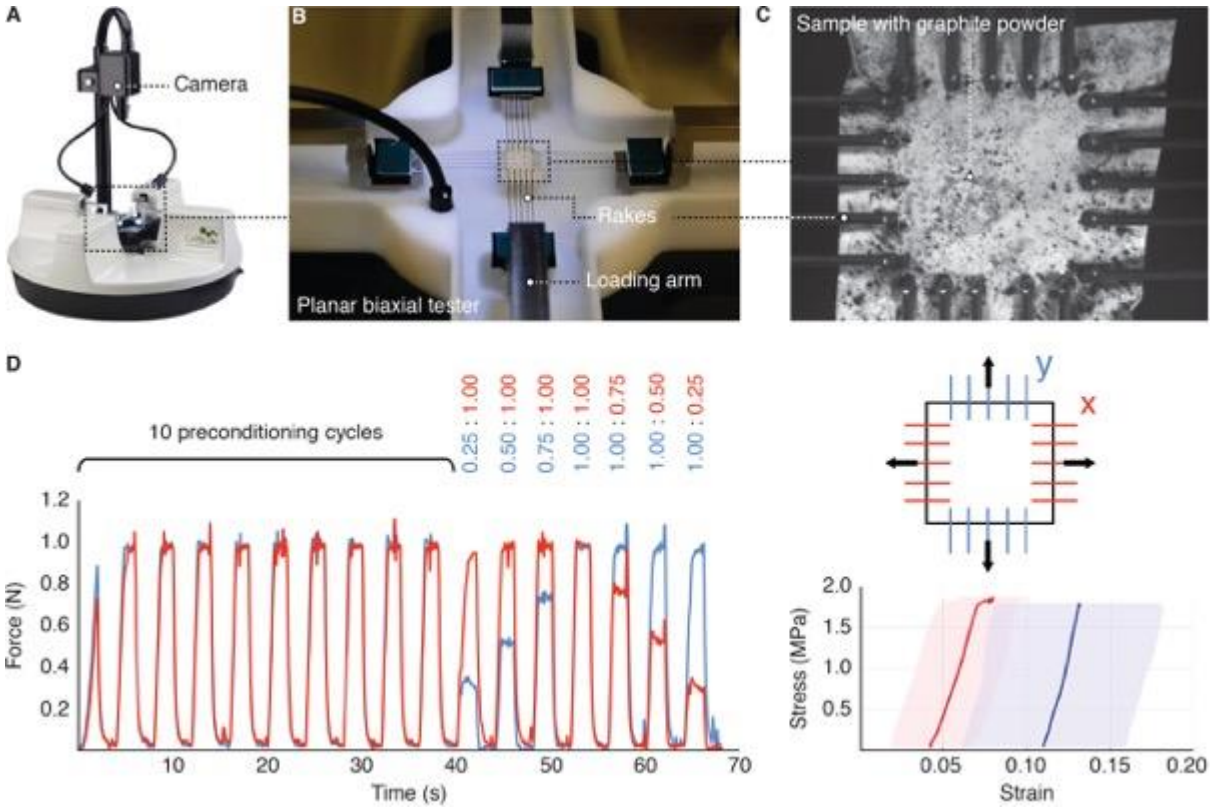

Fig S5: Experimental setup for biaxial testing of 0.1 mm ePTFE leaflet material. (**A** and **B**) Biaxial testing machine and details of loading assembly and tungsten rakes. (**C**) View of a 0.1 mm thickness ePTFE (Goretex) sample being tested. Cartesian coordinate system indicates positioning of sample based on principal material direction. (**D**) Force-controlled test protocol for assessment of biaxial strain. Corresponding stress-strain plot for 0.1 mm thickness ePTFE (Goretex) at 1 N equibiaxial loading. Stress is represented using second Piola-Kirchhoff membrane tension (N/m), strain is based on Green strain, and the shaded bands indicate (+/- 2 STD).

Fabrication of functional valve samples

Valve samples were fabricated based on the leaflet profile geometry and leaflet attachment geometry methodologies described above. In order to fabricate working valve samples, manufacturable leaflet attachment frames were designed using CAD software. Leaflet attachment were then generated using a sweep featured that combined the 3-D leaflet attachment curve and a circular cross section (Ø2.5 mm) to generate a solid volume that could be fabricated via additive manufacturing. The leaflet attachment geometry was based on the inner diameter of the frame samples to ensure that the H/D ratio was representative of the leaflet attachment location irrespective of the frame thickness (fig. S6). A series of holes were patterned along the swept feature to allow leaflets to be physically sewn into the leaflet attachment frame. During the early design stages, sequential prototype evaluation was performed using models fabricated with a Form2 stereolithography-based 3D printer (FormLabs, Somerville, MA, USA), using their RS-F2-TOTL-05 (Tough) resin. Once a final geometry had been identified, subsequent physical prototypes were fabricated from

ASTMF1537-11 cobalt chrome using direct metal laser sintering additive manufacturing (MLab, Concept Laser GmbH, Lichtenfels, Germany).

Leaflets were cut from a 0.1 mm thickness sheet of ePTFE (Gore® Preclude® pericardial membrane, W. L. Gore & Associates, Flagstaff, AZ USA) using surgical scissors and a guiding template. The leaflets were cut out such that the most extensible material orientation was oriented parallel to the long axis of the leaflet (fig. S6).

Leaflets were sewn into the leaflet attachment frame with a running stitch. The leaflets were initially sewn at the commissure and valve base locations to ensure correct alignment. Finally, the assembled valve samples were placed inside flexible polyurethane tubing (Tygon, Saint-Gobain, Courbevoie, France). A thin film of sealant (Sil-poxy^{TM}) was manually applied to the underside of the leaflet attachment frames to ensure no paravalvular leakage during hydrodynamic testing.

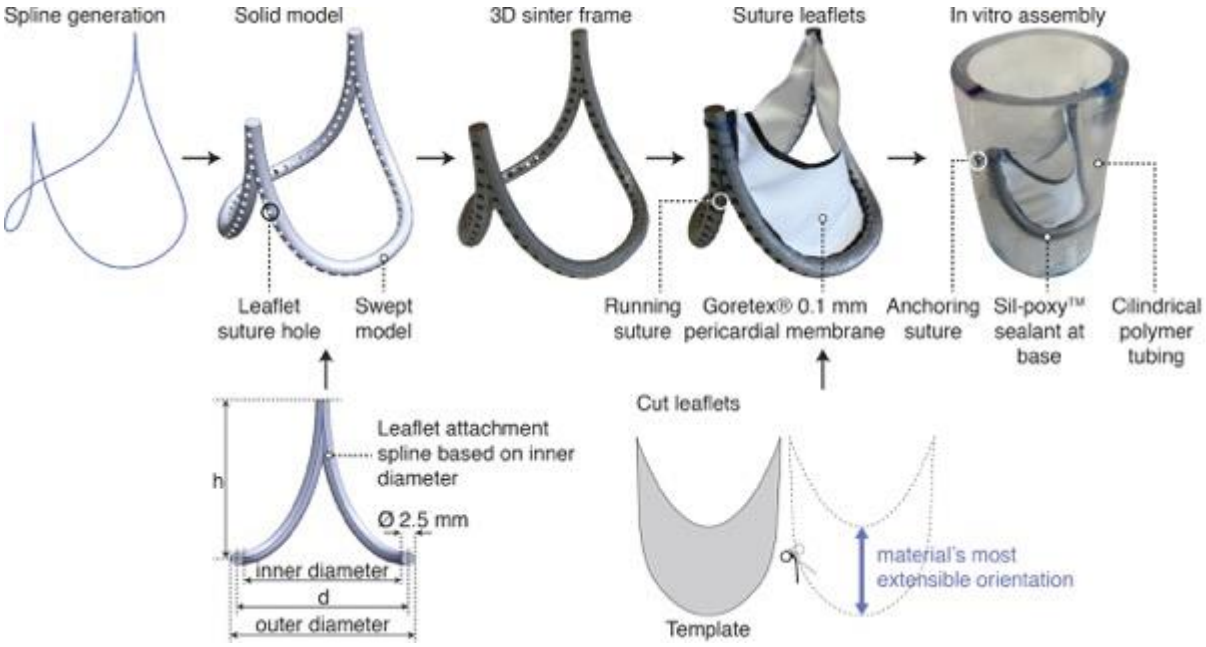

Fig S6: Fabrication of primary biomimetic valve prototype for *in vitro* testing. Methodology for creating a sample of the primary biomimetic valve geometry, from initial geometric definition through to a physical embodiment for *in vitro* testing.

In vitro hydrodynamic testing

Benchtop hydrodynamic performance testing was used to determine whether our biomimetic bileaflet valve design with 1) fixed leaflet attachment perimeter length and 2) fixed leaflet profile geometry, could function effectively with diametric expansion. A comprehensive series of experiments were performed to characterize transvalvular pressure gradient (pressure drop), effective orifice area, and valve regurgitation over a wide range of physiologic and supraphysiologic flow and pressure conditions.

Flow loop apparatus

Valve prototypes were tested in a pulsatile flow loop apparatus (ViVitro Labs Inc, Victoria, BC Canada). This system complies with ISO standards for surgical cardiac valve prostheses (ISO 5840-2:2015) and transcatheter valves (ISO 5840-3:2013). The flow loop system (fig. S7) was powered by a volume-displacement piston pump (Superpump, ViVitro Labs Inc, Victoria, BC Canada) to simulate cardiac output. A mixture of 0.9 ± 0.2 % sodium chloride in glycerin and distilled water blood analog solution with a viscosity of 3.0 ± 0.5 cP (0.5 ± 0.5 mL of Cosmocil® (Londa, Basel, Switzerland) per 1L) was used as a working fluid to emulate blood.

The pump displaced the working fluid into a chamber that incorporated a sealed silicone ventricular sac, causing compression of the ventricular sac to mimic cardiac muscle function. Repeated compression and distention of the ventricular sac generated a pulsatile flow in the flow loop apparatus. A reservoir emulating the right atrium was connected to the ventricular sac, and a one-way mechanical valve at this inlet was utilized to mimic the atrioventricular valve (mitral/tricuspid valves). A pressure transducer (HCM018, ViVitro Labs Inc, Victoria, BC Canada) was mounted in the atrial reservoir to monitor atrial pressure. An outlet chamber from the ventricular sac provided the testing chamber for the valve prototype. A pressure transducer (HCM018, ViVitro Labs Inc, Victoria, BC Canada) and electromagnetic flow probe (EP688, Carolina Medical, East Bend NC) were mounted proximal to where the valve prototype was mounted. A second pressure transducer (HCM018, ViVitro Labs Inc, Victoria, BC Canada) was mounted distal to the valve prototype. High frame rate cameras (Photron SA3 60K M2, San Diego, CA) were used to image the valve prototypes in the transverse plane and from a plan view at a rate of 1000 fps. The working fluid was pumped from the ventricular sac, through the prototype valve, then looped back to the atrial reservoir via a network of tubing that had adjustable hydrodynamic resistance to represent the body. Air volumes were used to add compliance to an otherwise rigid system to replicate anatomical compliance. Fluid was regulated at 37+/-0.1 °C using a heat exchanger system. The pumping parameters were adjusted by a control system to allow systematic testing of valve prototypes and specific hemodynamic conditions. The target forward flow volume per cycle, beat rate and systolic duration period (as a fraction of a cardiac cycle) were each adjustable. The systolic and diastolic arterial pressures were also adjusted; similarly, the back pressure on the valve prototype was adjustable by changing the peripheral resistance and compliance volumes. Experimental data was processed by a data acquisition system (ViViTest, ViVitro Labs Inc, Victoria, BC Canada) at a rate of 256 samples per beat (60 beats/min sampling is 256 Hz and 150 beats min is 102 Hz).

Output metrics

The purpose of these *in vitro* experiments was to quantitatively assess transvalvular pressure gradients (pressure drop across the valve), effective orifice area (EOA), and valve regurgitation for the geometrically accommodating bileaflet valve design.

The second output metric of interest is the peak-to-peak transvalvular pressure gradient. This is defined as the pressure difference between the ventricular peak pressure and the arterial peak pressure (i.e peak pressure downstream of valve). This pressure metric is of interest because it provides quantification of valve function in allowing unimpeded forward flow, i.e it is an indication of heart valve efficiency.

We also assessed the effective orifice area of each valve sample during operation to assess how effectively the biomimetic valve design accommodates radial expansion without obstructing forward flow. The EOA provides an index of how well a valve design utilizes its internal stent orifice area. An effective orifice area was computed using a 1D incompressible, steady-state fluid flow model, defined as:

$$\text{EOA } (cm^2) = \frac{Qrms}{51.6\sqrt{\frac{\Delta P}{\rho}}}$$

Where Q_{rms} is the root mean square systolic/diastolic flow rate (cm^3/s), ΔP is the mean systolic/diastolic pressure drop (mmHg), and ρ is the working fluid density.

Valve regurgitation is a metric of interest because it demonstrates the extent to which a valve obviates reverse flow and effectively acts as a one-way valve. Valve regurgitation was quantified in absolute terms as a volume of regurgitant flow, which incorporates the sum of the valve closing volume and the valve leakage volume. Valve closing volume is defined as the volume of reverse flow through the valve during valve closure, and valve leakage volume represents the volume of reverse fluid flow that occurs through the valve after valve closure. Valve regurgitation was also considered in relative terms, as a % fraction of fluid forward flow through the valve.

For each test condition, output metrics were acquired for a total of 10 consecutive cardiac cycles at steady-state conditions.

Experimental variables

The primary dependent variables in these *in vitro* characterization studies were the expanding valve geometry from an initial baseline valve diameter and the initial H/D ratio. A series of 11 samples were fabricated in total using the methods described above. An initial 5 samples were fabricated with a baseline H/D=1.7 and baseline internal diameter (ID) of 16 mm. Valve prototypes were fabricated at baseline (1X) and expanded dimensions in +20% increments up to 1.8X diameter, with the following dimensions: 16 mm (baseline), 19.2, 22.4, 25.6, and 28.8 mm. A further 6 samples of baseline H/D=2 and 16 mm baseline ID were also fabricated at +20% increments (diameters of 16 mm, 19.2, 22.4, 25.6, 28.8 mm and 32 mm). These particular valve sample diameters and increments were chosen to match standardized flexible polymer tubing diameters compatible with the experimental flow loop apparatus. For each expanding series of valve prototypes, the leaflet profile geometry sewn into each leaflet attachment frame was identical to mimic a non-growing leaflet. The leaflet profile geometry for each series of samples was defined by the baseline valve H/D ratio.

For each valve sample of a given geometry and dimension, we further manipulated key hydrodynamic input parameters to characterize each sample across a range of physiological and super-physiological conditions. Since the primary objective of the size-adjustable biomimetic bileaflet valve design was to successfully accommodate diametric vessel growth without loss of function, we derived hemodynamic flow rates appropriate for each valve sample according to its diameter. Since cardiac output (blood flow rate) varies considerably between humans of different ages (and thus valves of different diameter), we characterized samples by maintaining a constant cardiac index. Cardiac index is a hemodynamic parameter that relates

the cardiac output to the size of an individual with respect to body surface area. To calculate the cardiac output for a given valve diameter, we obtained an average body surface area for the relevant valve diameter using clinical data (*23, 56*). Secondly, we computed the cardiac output for a given valve diameter from the estimated body surface area and a target cardiac index.

To assess the transvalvular pressure gradient (pressure drop) and the effective orifice area across each valve dimension, we assessed 3 cardiac indices: 2.5, 3.0 and 3.5 to represent a broad physiologic range. During each test, we fixed the systolic duration period to 45% (+/-5%); Pressures were adjusted to assess valve performance under right and left heart conditions; mean arterial pressure ranged from 20 mmHg to 100 mmHg, systolic arterial pressure ranged from 25 mmHg to 200 mmHg, and diastolic arterial pressure ranged from 10 to 160 mmHg. Beat rates ranged from 60 to 150 bpm.

To assess valve regurgitation, we fixed the cardiac index to be 3.0. For each valve sample, we varied both the heart rate (60, 80 and 150 bpm) and the back pressure on the valve (5, 10, 20, 50 80, 160 mmHg). During these tests we fixed the systolic duration period to be 45% of the cardiac cycle (+/-5%).

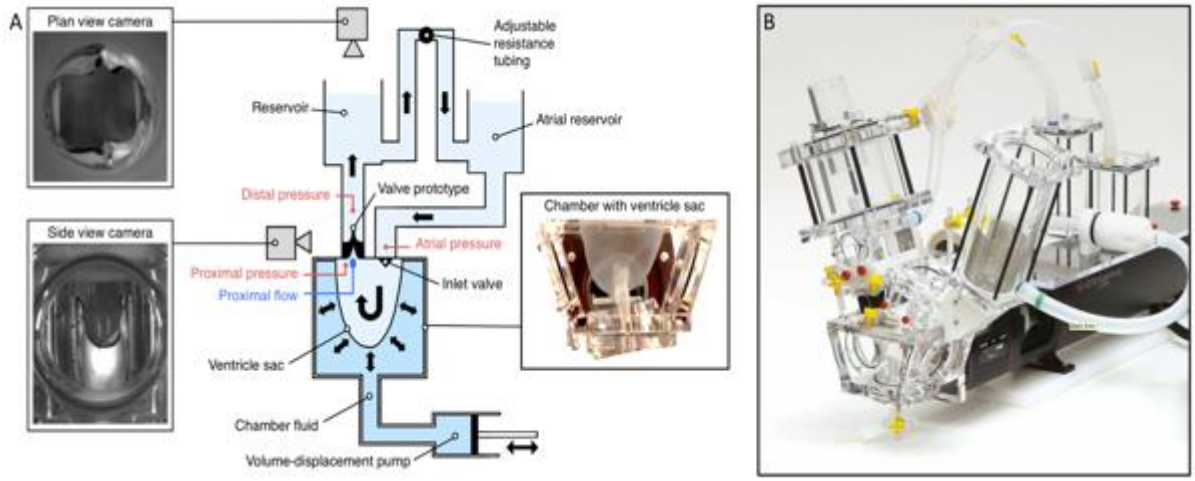

Fig S7: *In vitro* circulatory flow loop system (A) schematic representation of the *in vitro* flow loop apparatus and **(B)** photograph of the *in vitro* flow loop apparatus (ViVitro Labs Inc, Victoria, BC Canada).

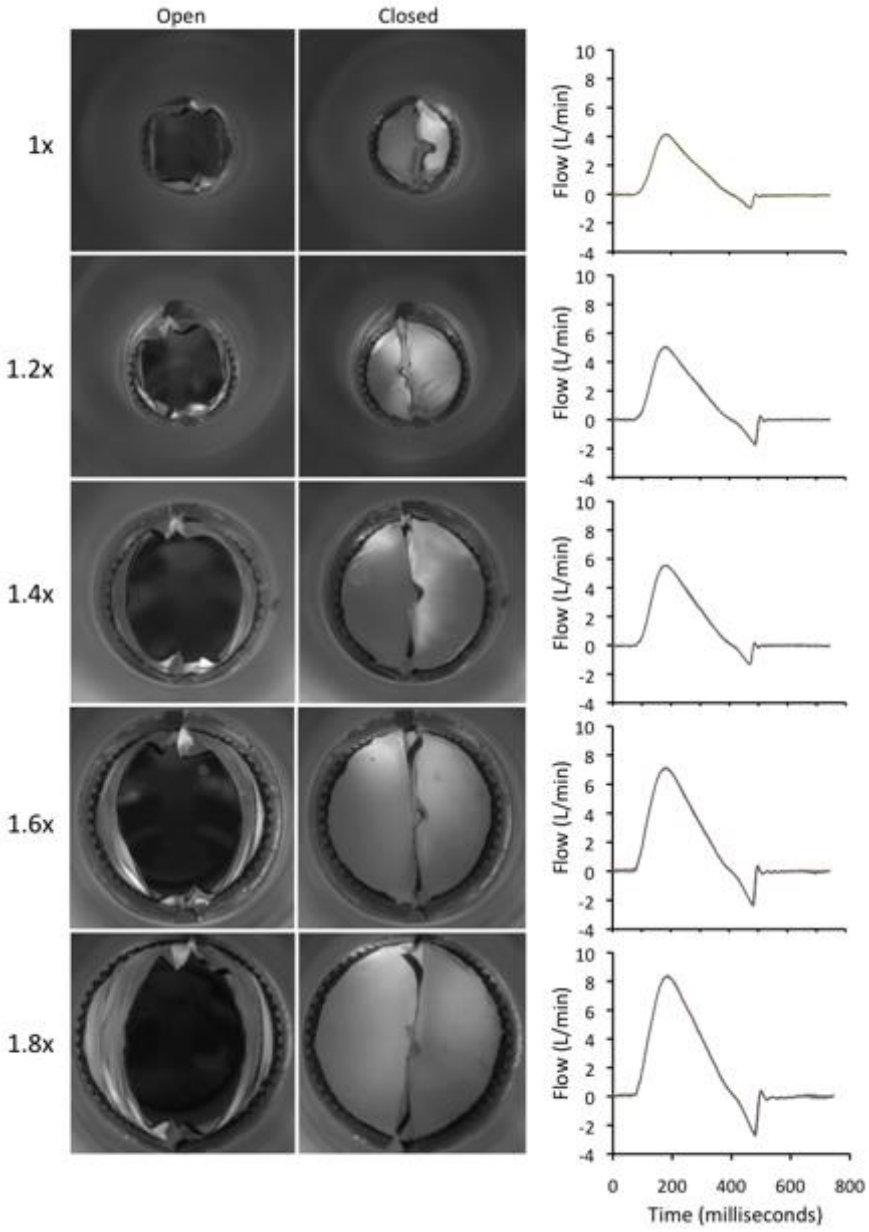

Fig. S8: *In vitro* flow loop testing data: primary valve geometry. (**Left)** Photographs of valve prototype at increasing states of expansion (1X up to 1.8X), shown in systole (open valve) and diastole (closed valve). **(Right)** Flow profiles for each valve diameter tested at a cardiac index of 3.0, beat rates/min: 80, systolic duration: 45%. Each plot shows the flow waveform recorded over 10 consecutive cycles, which are overlaid to demonstrate repeatability.

Finite element modeling

In this section, we describe the construction and processing of the Finite Element Analysis (FEA) performed to evaluate the magnitude and distribution of stresses on the geometrically accommodating valve leaflet in a quasi-static, closed position (diastole). The leaflet-stent

model was constructed using the commercial Computer Aided Design (CAD) software SolidWorks (by Dassault Systèmes, Waltham, MA, USA) and was designed to precisely match the geometry of the experimental setup. Separate CADs for the leaflet and the different expansion geometry stents were generated. The FEA simulations were performed using the commercial solver ABAQUS/Explicit 2017 (by Dassault Systèmes, Waltham, MA, USA). The stent geometry was assumed to be a non-deformable rigid material with a set of displacement conditions imposed to simulate the transition between the different expansion states. The leaflet geometry was modeled using 3D deformable elements (C3D8R - 8-node hexahedral brick general-purpose continuum elements with reduced integration for finite membrane strains) with TIE constraints imposed on the nodes located along the perimeter of the leaflet. These constraints connect the leaflet to the stent geometry. The mesh size for the leaflet is chosen to remain smaller than 0.4 mm anywhere within the leaflet domain. A general contact condition is defined between all nodes interacting with each other.

The constitutive model used is set to match the material properties of 0.1 mm thickness ePTFE - Goretex pericardial membrane (W.L Gore and Associates, Inc., Arizona, USA), which satisfies an isotropic hyperelastic Marlow material. For this material model, the strain energy potential is described by $U = U_{dev}(\bar{I}_1) + U_{vol}(J_{el})$, where U is the strain energy per unit of reference volume, with U_{dev} as its deviatoric part and U_{vol} as its volumetric part; $\bar{I}_1$ is the first deviatoric strain invariant and J_{el} is the elastic volume ratio. We obtained the parameters for this material model by fitting the model to the experimental data. We chose our material model to be within 2 standard deviations of the most compliant material direction to match the physical deformation of the valve leaflets observed under *in vitro* flow loop testing conditions. This was chosen with the rationale to provide the most appropriate isotropic measure given that the experimental leaflet had the more compliant Goretex material direction aligned with the direction of largest strain. Additionally, to create a computationally efficient model, we used mass-scaling to arrive at the desired quasi-static solution while introducing negligible numerical errors.

The FEA model is subdivided into two sequential steps: the first step expands the base geometry stent to achieve the desired expansion state. This step is performed by creating a map between the different expansion states and applying a smooth expansion transition between the different states. A map is created that relates the transition for each node from its original state to its expanded state. This map is then applied as a displacement condition for each of the nodes. Once the final desired expansion configuration is achieved, a subsequent step applies the pressure boundary condition on the leaflet. The negative pressure conditions are imposed along the outflow surface of the leaflets, leading the leaflets to close and interact. The pressure step is slowly imposed as a ramping step in an effort to minimize the kinematics of the model and efficiently arrive at the steady-state, quasi-static solution. For each FEA simulation, the model is simulated long enough to ensure the correct quasi-static deformation solution matching the experimental deformation is achieved. Furthermore, a calibrated damping coefficient is applied to minimize numerical kinematics resulting from the model's inertia.

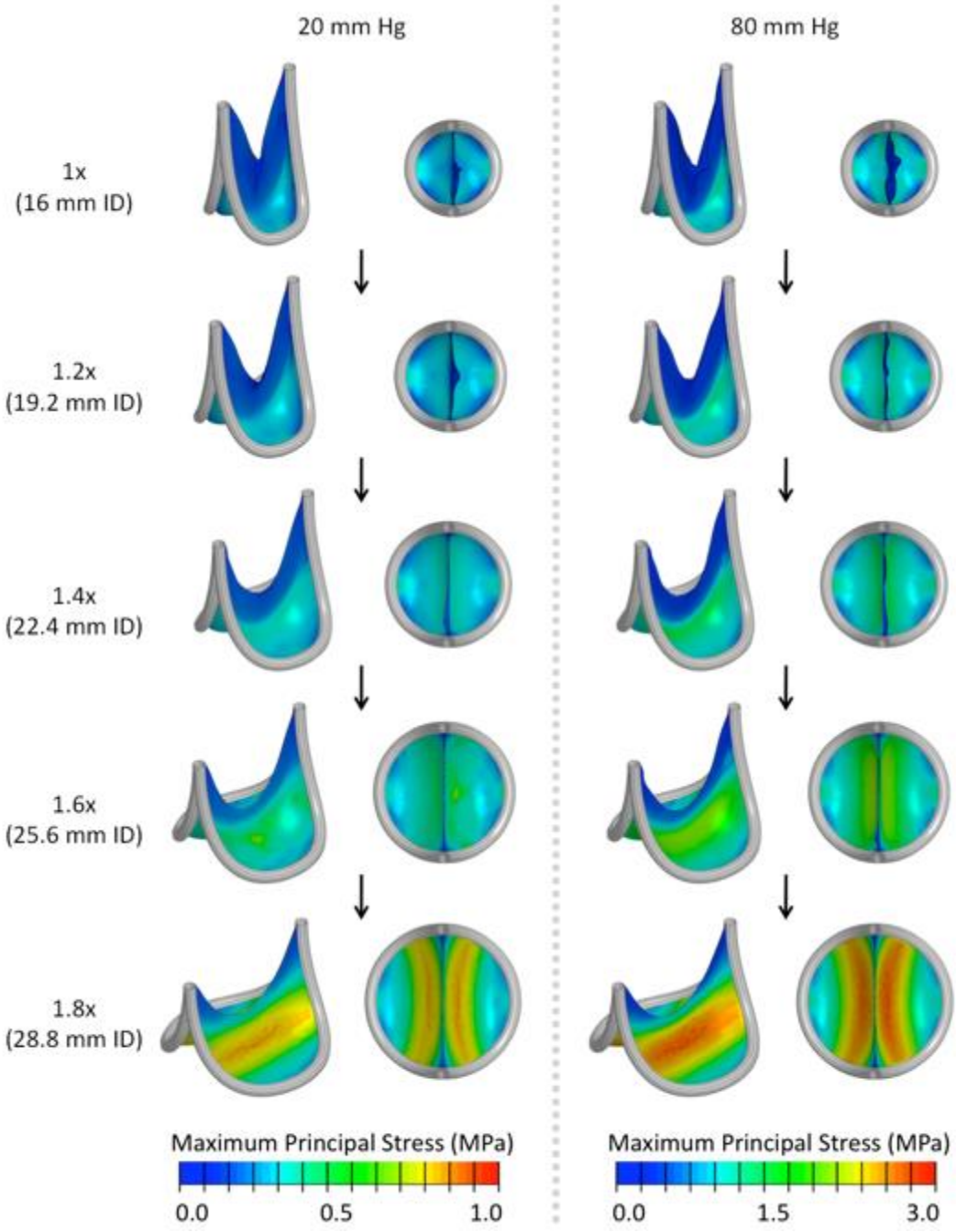

Fig. S9. Finite element model of leaflet stresses in quasi-static loaded state under right and left heart loading conditions. Leaflet material is 0.1 mm thickness ePTFE (Goretex, W.L Gore and Associates, Inc., Arizona, USA). Results shown are simulated under right heart (20 mmHg, left panel), and left heart (80 mmHg, right panel) loads. All plots are based on the same scale of maximum principal stress, ranging between 0 to 1 MPa and 0 to 3 MPa for right and left heart loads, respectively.

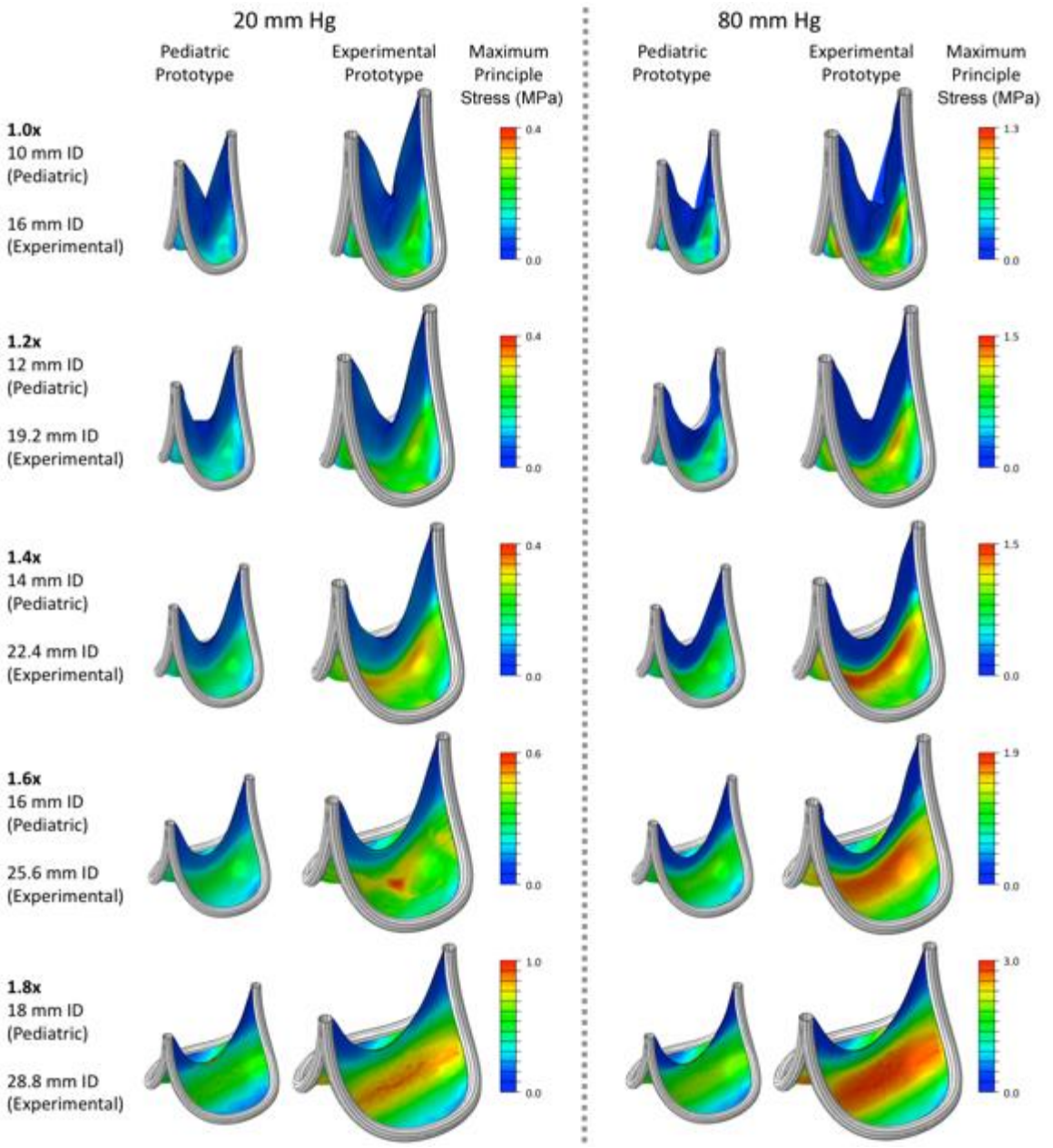

Fig. S10. Finite element model of leaflet stresses in quasi-static loaded state under right and left heart conditions - pediatric dimensions (baseline valve diameter = 10mm). Leaflet material is 0.1 mm thickness ePTFE (Goretex, W.L Gore and Associates, Inc., Arizona, USA). Results shown are simulated under right heart (20 mmHg, left panel), and left heart (80 mmHg, right panel) loads. All plots are based on the same scale of maximum principal stress, ranging between 0 to 1 MPa and 0 to 3 MPa for right and left heart loads, respectively.

In vivo acute ovine studies: functional assessment of primary biomimetic valve geometry

We performed acute i*n vivo* studies in juvenile sheep to evaluate the functional performance of the primary biomimetic valve geometry. The animal experiments were conducted in full compliance with the 1996 Guide for the Care and Use of Laboratory Animals recommended by the U.S. National Institutes of Health. All acute *in vivo* studies were performed at Boston Children's Hospital. The experimental protocol was approved by the hospital's Institutional Animal Care and Use Committee.

Polymer-based prototypes of the primary valve geometry were fabricated using stereolithography additive manufacturing (Somos→ perFORM, DSM Functional Materials, Elgin, Illinois, USA), which was performed to enable artefact-free echocardiography of the device. Reinforcement features were added to the prototypes to increase the rigidity of the polymer valve frame. The valve samples generated for *in vivo* testing were equivalent geometry and dimensions to the *in vitro* samples tested and were generated using the same methods as previously described.

To determine *in vivo* functionality of the primary biomimetic valve geometry we tested the two polar states of valve expansion (i.e. 1X and 1.8X). A total of 8 polymer-based prototypes were produced. Four valves were fabricated with baseline H/D ratio of 1.7:1, and 14 mm internal diameter (ID) and four valves were fabricated with a 1.8X expanded diameter from these baseline dimensions (i.e valve ID = 25 mm). To facilitate surgical implantation, a sleeve/sewing cuff was constructed using Goretex vascular graft (W.L Gore and Associates, Inc., Arizona, USA).

Procedure

Female Dorset lambs (N = 4, mean weight 20.9 ± 2.2 kg, Parsons EM and Sons Inc.) and female Dorset sheep (N = 4, mean weight 58.1 ± 2.7kg, Parsons EM and Sons Inc.) were used. Animals were anesthetized using intravenous (IV) Ketamine (10 mg/kg), versed (0.1 mg/kg) and intramuscular injection (IM) of atropine (0.04 mg/kg). The animals were intubated with a cuffed endotracheal tube and mechanically ventilated with volume-control mode (Fabius Tiro; Draeger Medical, Andover, MA). Anesthesia was maintained with inhaled desflurane (8-12%). A transurethral urinary catheter was placed for monitoring urine output. Arterial and central venous lines were placed percutaneously in the femoral artery and external jugular vein for arterial and central venous pressure monitoring, respectively. Electrocardiogram monitoring was achieved using an esophageal probe and temperature was monitored via rectal probe placement. The neck, chest and groin were disinfected using povidone-iodine and alcohol solutions.

Access to the heart and pulmonary valve was achieved by performing a left-sided thoracotomy in the 4th intercostal space, and external measurements of the pulmonary valve annulus diameter and main pulmonary artery length were performed. Baseline hemodynamic data was obtained via placement of right ventricular and pulmonary artery pressure lines and a perivascular flow probe (Transonics, TS420) around the distal main pulmonary artery. Baseline 2-D epicardial echocardiography was performed using a matrix array ultrasound probe X7-2 (2-7 MHz) on an iE33 system (Philips Healthcare) to measure the native pulmonary valve annulus diameter, main pulmonary artery length (defined as the linear distance between the

pulmonary valve annulus and bifurcation of the branch pulmonary arteries) and assess overall heart function. After intravenous heparin (300 IU/kg) was administered to achieve an activated clotting time of >350 seconds, arterial cannulation was performed via the ascending aorta and venous cannulation was performed via the right atrial appendage. Cardiopulmonary bypass was initiated using an oxygenator (FX15 or FX25, Terumo Medical Corporation). Isoflurane (1-4%) was administered for maintenance of anesthesia during cardiopulmonary bypass. With the animal cooled to 33°C and under beating-heart conditions, a longitudinal incision was made along the anterior aspect of the main pulmonary artery, extending to just below the level of the pulmonary valve annulus. The native pulmonary valve leaflets were then excised. Next, depending on the animal size, we implanted either a 14 mm or 25 mm internal diameter valve prototype in the native pulmonary valve position. This was performed using interrupted 4-0 Prolene sutures, placed in a circumferential fashion. After valve implantation, the pulmonary artery was closed, and hemostasis was obtained. Animals were then weaned off cardiopulmonary bypass and arterial and venous cannulas were removed. Animals were observed for 4 to 6 hours post wean from cardiopulmonary bypass. 2-D epicardial echocardiography, including color and continuous wave Doppler imaging, and 3-D echocardiography was performed at 1- and 4-hours post implantation to evaluate valve function. Continuous monitoring of right ventricular and pulmonary artery pressures, and main pulmonary artery flow were also performed throughout the observation period to assess valve hemodynamic performance and overall heart function. At the conclusion of the study, animals were euthanized by intravenous injection of overdosed pentobarbital sodium (Fatal-Plus®, 86 mg/kg). The heart was then excised and opened for direct inspection of the valve.

Data Analysis

The flow and pressure data were logged using an acquisition system (Powerlab, AD Instruments, New Zealand) at a rate of 10 kHz. Flow and pressure data were analyzed using data analysis software (LabChart, AD Instruments, New Zealand). To assess valve regurgitation, we integrated the flow rate to obtain a forward flow volume, a closing volume and valve leakage volume. The total regurgitant volume (closing and leakage volumes) was then expressed as a % of the forward flow volume. Transvalvular pressure gradient was computed from the measured right ventricle and PA pressures (right ventricular pressure – PA pressure). Peak-to-peak transvalvular pressure gradient values was computed during the forward flow phase.

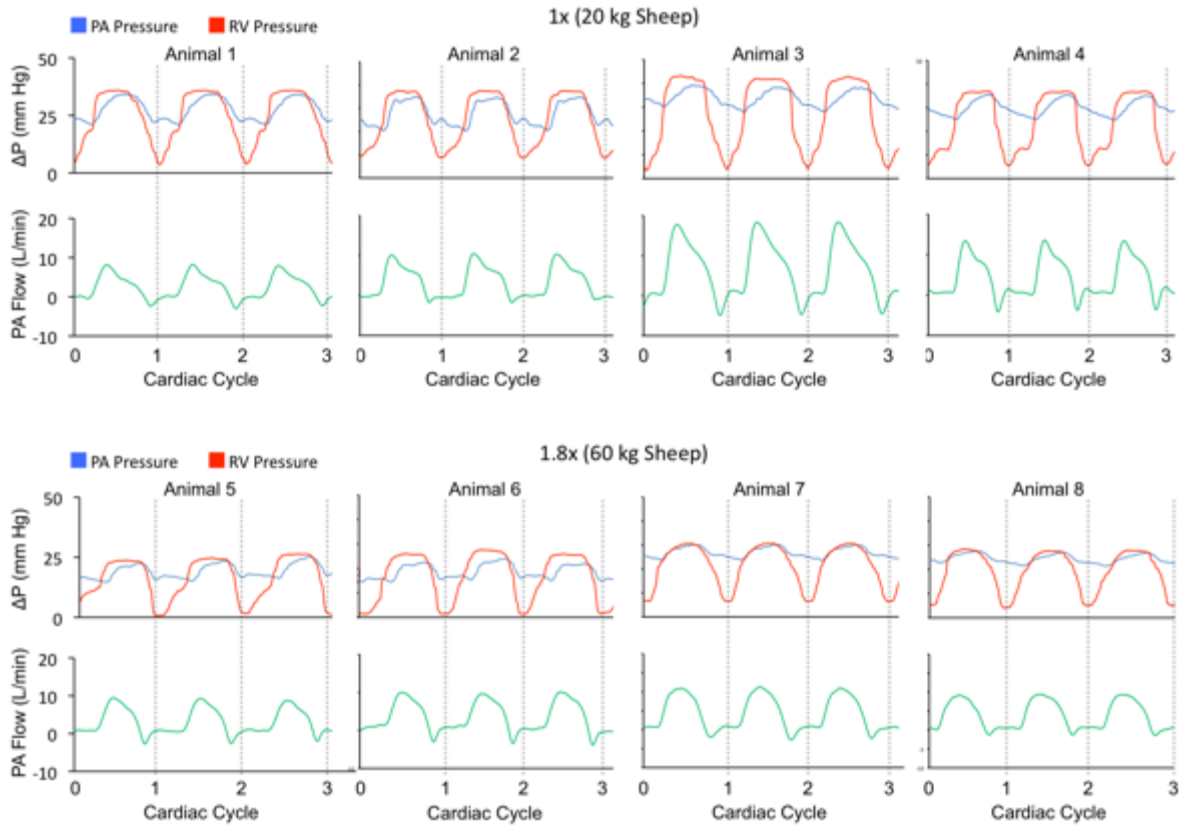

Fig. S11: Acute *in vivo* studies in juvenile and adult sheep: Representative hemodynamic data. Representative *in vivo* data obtained from all 8 study animals showing transvalvular (⊗P) pressure gradient and pulmonary artery flow for the 1X and 1.8X expanded valve geometries, respectively. RV = right ventricular, PA = pulmonary artery.

Table S2: Peak-to-peak transvalvular pressure gradient for 1X valve geometry in 4 animals. Data based on n = 10 consecutive cardiac cycles at ~2 hours post device implant.

	Mean (mmHg)	Standard deviation (mmHg)
Study 1	1.5	0.4
Study 2	2.9	0.3
Study 3	3.1	0.7
Study 4	0.9	0.5

Table S3: Peak-to-peak transvalvular pressure gradient for 1.8X expanded valve geometry in 4 animals. Data based on n = 10 consecutive cardiac cycles at ~2 hours post device implant.

	Mean	Standard deviation
Study 1	10.3%	2.2%
Study 2	11.3%	1.6%
Study 3	7.0%	0.8%
Study 4	5.8%	0.7%

Table S4: Regurgitant fraction for 1X valve geometry in 4 animals. Data based on n = 10 consecutive cardiac cycles at ~2 hours post device implant

	Mean	Standard deviation
Study 1	5.3%	0.8%
Study 2	7.9%	2.0%
Study 3	4.7%	1.3%
Study 4	4.4%	1.3%

Table S5: Regurgitant fraction for 1.8X expanded valve geometry in 4 animals. Data based on n = 10 consecutive cardiac cycles at ~2 hours post device implant.

	Mean (mmHg)	Standard deviation (mmHg)
Study 1	1.5	0.2
Study 2	3.8	0.2
Study 3	0.6	0.3
Study 4	1.3	0.2

In vivo acute ovine study: Biomimetic valve implantation in native aortic valve position

For proof of concept, we also conducted acute, non-survival experiments to implant the biomimetic valve prototype in the native aortic valve position of juvenile sheep (N = 2). The goal was to assess mechanical and hemodynamic performance of the biomimetic valve in the left-sided systemic semilunar valve position. The experimental protocol for these experiments was identical to the acute, non-survival pulmonary valve implants.

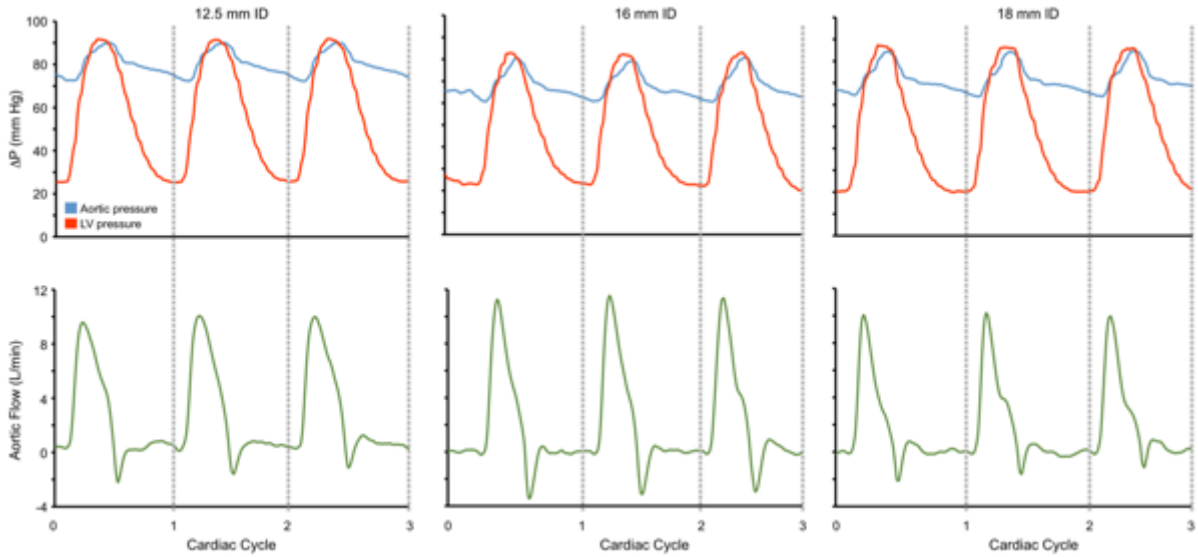

Fig. S12. ***In vivo*** **validation of biomimetic valve performance in the native aortic valve position: acute studies in juvenile sheep.** Representative *in vivo* data obtained from one study animals demonstrating transvalvular (ΔP) pressure gradient and ascending aorta flow for the 12.5 mm ID, 16 mm ID and 18 mm ID expansion states, respectively. LV = left ventricle.

Expandable biomimetic valve prototype: *in vitro* expansion and hydrodynamic testing

Biomimetic expandable valve prototypes were fabricated using 0.1mm ePTFE for leaflet material and a laser-cut stainless-steel frame (Fig. S13). Fabricated valves were sequentially balloon dilated on the benchtop from 12.5 mm (1X) up to 23 mm (1.8X) (Fig. S13). These prototypes were then tested at 4 states of expansion (12.5 mm ID, 16 mm ID, 20 mm ID and 23 mm ID) in the aforementioned pulsatile flow loop system (Vivitro Labs, pulse duplicator). The purpose of these *in vitro* experiments was to quantitatively assess transvalvular pressure gradient (ΔP), effective orifice area (EOA), and degree of valve regurgitation across all expansion states from 1X to 1.8X diameter for the expandable prototype design.

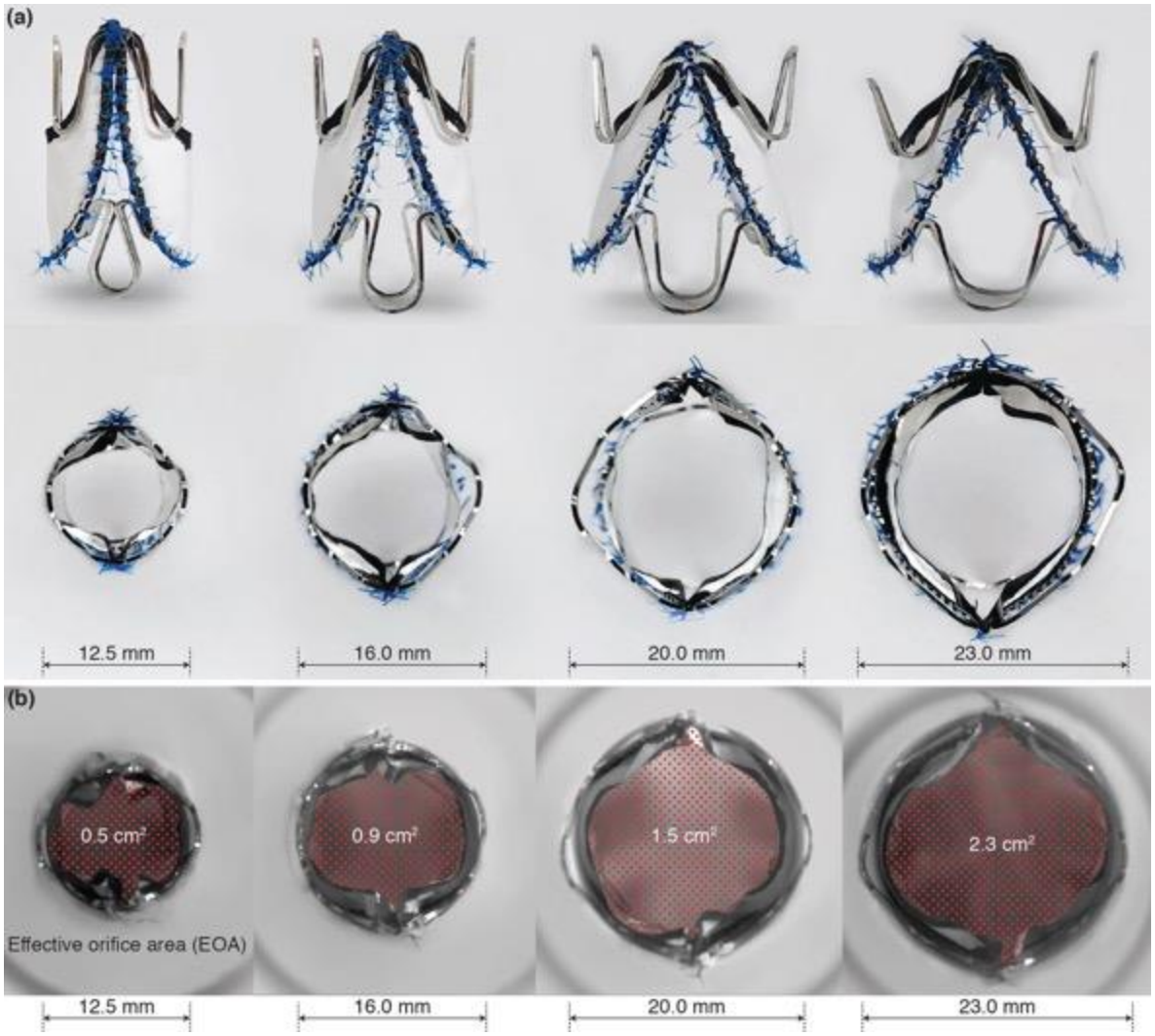

Fig. S13: **Expandable biomimetic valve prototype: frame expansion profile and leaflet opening function. (A)** Side view photographs of fabricated expandable biomimetic valve prototype, with 0.1 mm thick ePTFE leaflets sewn to the stainless-steel stent. Photographs show serial expansion of valve from 12.5 mm ID (1X) to 23 mm ID (1.8X). (**B**) Corresponding top view images of valve outflow surface from 1X to 1.8X diameter. (**C**) Photographs of valves being testing in *in vitro* flow loop system. Leaflets are in the open position, and the red dots indicate effective orifice area of valve at each stage of expansion. Effective orifice area (EOA, cm^2) = Qrms / (51.6 $\sqrt{(\Delta P/\rho)}$).

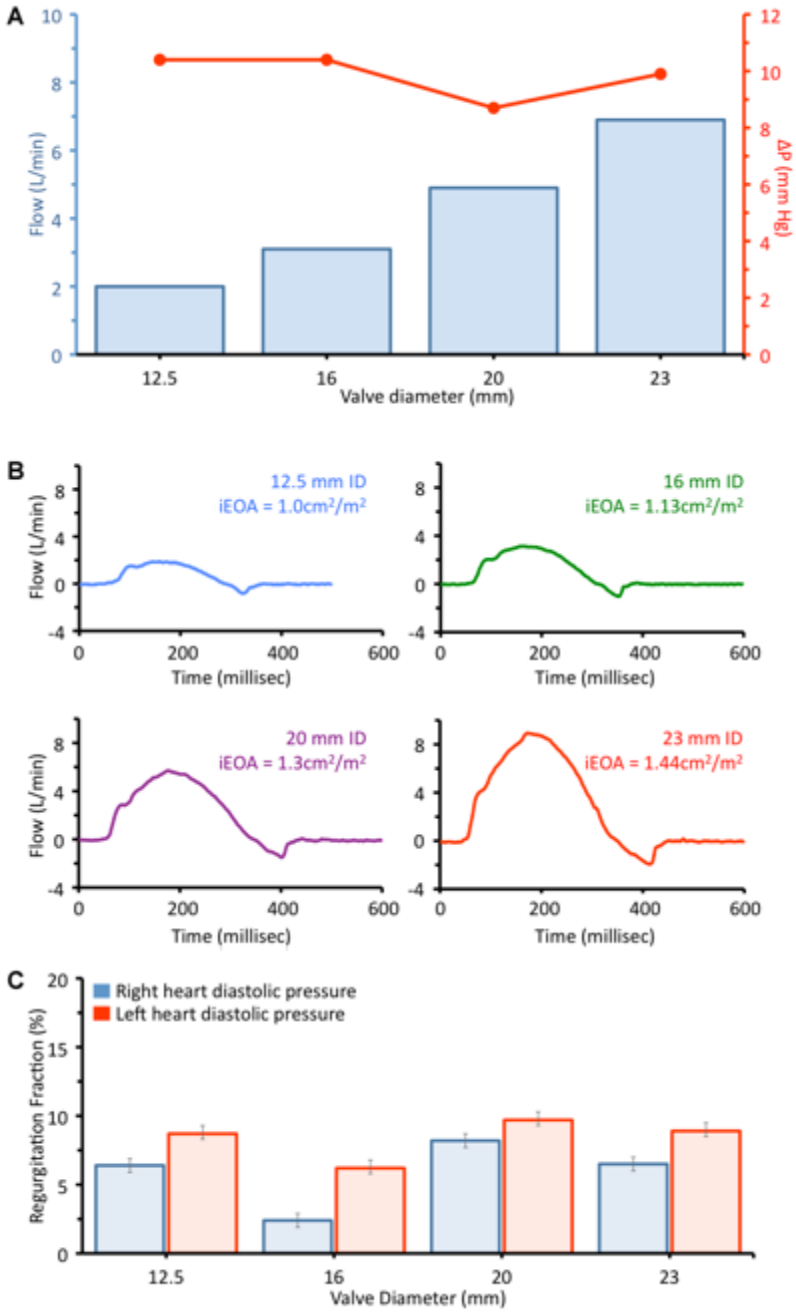

Fig. S14. *In vitro* characterization of the biomimetic expandable valve: flow loop testing. **(A, B, C)** Expandable valve prototype was tested at different states of diametric expansion (1X to 1.84X) in an *in vitro* circulatory flow loop, under physiologic left and right heart conditions. **(A)** Mean transvalvular (ΔP) pressure gradient (red line) at each stage of valve expansion (1X to 1.84X). Flow is adjusted to match valve size and replicate the physiology of a growing child. **(B)** Four plots demonstrate flow profiles of the expanding valve geometry from 1X (12.5 mm ID) to 1.84X (23 mm ID). **(C)** Valve competence (closing function) under right (20 mmHg, blue bars) and left (80 mmHg, red bars) heart loads. Error bars represent ±1 standard deviation.

In vivo proof-of-concept of valve expansion: growing lamb model

Seven Polypay and Hampshire breed juvenile sheep (male and non-pregnant female) were included in this study (mean weight = 22.5 ± 0.9 kg, mean age = 9 ± 3 weeks). Experiments were conducted in compliance with the National Institutes of Health (NIH) Guide for the Care and Use of Laboratory Animals. All studies were conducted at the University of Minnesota, Experimental Surgical Services animal facility. The experimental protocol was approved by the University of Minnesota's Institutional Animal Care and Use Committee (1810A36420).

Valve implantation

The expandable biomimetic valve prototype (fig. S13) was implanted in all seven lambs, with a sleeve/sewing cuff constructed with Goretex vascular graft (W.L Gore and Associates, Inc., Arizona, USA) to facilitate surgical implantation. Each valve had a diameter of 12.5 mm at implantation.

All animals were acclimated in the holding facilities for a minimum of three days prior to study initiation. Solid food was withheld for 12 to 24 hours prior to surgery. Water was available at all times for fasting animals. Anesthesia was induced with propofol (2-6 mg/kg, intravenous), ketamine (10 mg/kg, intramuscular), and atropine (0.04 mg/kg, intramuscular). Animals were intubated post induction, and mechanical ventilation was initiated at 9-15 breaths per minute. Isoflurane (1-3%) was administered to maintain anesthesia. EKG monitoring leads were positioned on the animal's limbs. End tidal CO_2, oxygen saturation (Sp O_2), and temperature were monitored throughout the procedure. The chest was scrubbed with iodine surgical scrub, patted dry with sterile toweling, and sprayed with iodine/alcohol solution. Once the animal reached a deep plane of anesthesia, 0.4 to 0.8 mg/kg of intravenous succinylcholine chloride was administered. A left thoracotomy via the 4^{th} intercostal space was performed to access the heart and pulmonary valve. Next, the external pulmonary valve annulus diameter and main pulmonary artery length were measured. Baseline hemodynamic data were obtained via direct measurement of the right ventricular and pulmonary artery pressures and placement of a perivascular flow probe (Transonics, TS420) around the distal main pulmonary artery. Baseline 2-D epicardial echocardiography was performed to measure the native pulmonary valve annulus diameter and assess overall heart function. After administration of heparin (250 IU/kg), arterial and venous cannulation was performed via the descending thoracic aorta and right atrial appendage, respectively. Cardiopulmonary bypass was initiated, and the animal was gradually cooled to 28°C. Under beating heart conditions, the main pulmonary artery was opened to expose the pulmonary valve. The native pulmonary valve leaflets were excised and interrupted 4-0 Prolene sutures (Ethicon) were placed circumferentially into the native pulmonary valve annulus. The sutures were passed through the sewing skirt of the valve and the device was slid down the sutures using conventional surgical technique to implant the valve prototype in the native pulmonary valve position.

After valve implantation, the pulmonary artery was closed, and hemostasis was obtained. Animals were weaned off cardiopulmonary bypass and arterial and venous cannulas were removed. Once the animal was stabilized off cardiopulmonary bypass, protamine was administered at an approximate ratio of 1:1 (mL of protamine: mL of 1000 IU/ml heparin) for heparin reversal. 2-D epicardial echocardiography, including color and continuous wave Doppler echocardiography was performed to establish baseline post-operative valve function.

The pericardium was then approximated with one polyester suture. Prior to closing the thoracotomy, a local nerve block was introduced via intramuscular injection of lidocaine (1-2 mg/kg) and bupivacaine (1-2 mg/kg) at the incision site. The lungs were inflated and the chest cavity was irrigated with warm saline antibiotic solution (1 gram of ampicillin in 1 liter of sterile saline). A chest tube was placed for drainage and the chest incision was closed. Isoflurane was discontinued following closure of the thoracotomy. Animals were recovered in the OR, with all monitoring lines and chest tubes being removed prior to awakening from anesthesia. The endotracheal tube was removed once the animal had awakened. Once deemed stable, the animal was moved to the post-operative care area for further recovery. Post-operatively, animals received subcutaneous Heparin (1000 IU) once the evening of surgery and then twice daily for 5 days.

Serial transcatheter balloon dilation of valve implant

To accommodate somatic growth, the animals underwent transcatheter valve dilation procedures at predetermined time points during the survival period. At 2, 6- and 8-weeks post-implant, each animal underwent angiographic studies with transcatheter balloon dilation of the valve device. The extent of valve expansion was the same at each time point across all study animals; the valve was expanded to 16 mm ID at balloon dilation procedure 1 (2 weeks post implant), 18 mm ID at balloon dilation procedure 2 (6 weeks post implant), and 20 mm ID at balloon dilation procedure 3 (8 weeks post implant).

The animals were fasted for 12 to 24 hours (drinking water available at all times during fasting) in preparation for the valve dilation procedure. Anesthetic induction was achieved with propofol (2-6 mg/kg, intravenous), ketamine (10 mg/kg, intramuscular) and atropine (0.04 mg/kg, intramuscular). Animals were intubated post induction, and mechanical ventilation was initiated at 9-15 breaths per minute. Isoflurane (1-3%) was administered as needed to maintain deep anesthesia. EKG monitoring leads were positioned on the animal's limbs. End tidal CO_2, oxygen saturation (Sp O_2) and temperature were monitored throughout the procedure. Animals received one dose of intravenous ceftiofur (3 mg/kg) at the start of the procedure.

A small incision was made in the lateral neck to expose the right jugular vein and allow placement of a 14 Fr introducer sheath. Intravenous heparin (250 mg/kg) was administered and a Swan-Ganz catheter was inserted to measure transvalvular pressure gradient and cardiac output prior to valve dilation. To assess valve function, a pigtail catheter was inserted, and right ventricular and main pulmonary artery angiography was performed via injection of contrast and visualization under fluoroscopy. A guide wire was then introduced and an appropriately sized percutaneous balloon catheter (Atlas PTA Balloon Dilation Catheter, Bard Peripheral Vascular Inc., Tempe, AZ, USA) was advanced into position across the valve device. Under direct fluoroscopic visualization, the balloon was inflated to a nominal pressure of 6 atmospheres to expand the valve. Two dilations were generally performed, with the balloon first positioned distally and then proximally along the length of the device to ensure symmetric valve expansion. Valve performance and heart function were assessed post-dilation via right ventricular and main pulmonary artery angiogram and repeat measurement of transvalvular pressure gradient and cardiac output. Once data collection was completed, the introducer sheath was removed from the jugular vein and the incision was closed. Protamine (intravenous, 1mL: 1mL heparin) was administered at the end of the procedure. After each valve dilation, animals received short-term anticoagulation with one dose of subcutaneous Heparin (1000 IU) administered the evening of the procedure and twice daily administration for two days thereafter.

Table S6: *In vivo* hemodynamic data for 7 survival study animals at four separate time points. BD = valve balloon dilation. BD 1 = 12.5mm to 16mm ID (2 weeks post implant), BD 2 = 16mm to 18mm ID (6 weeks post implant), BD 3 = 18mm to 20mm ID (8-9 weeks post implant), Term = one-week post BD 3.

		Pre-dilation hemodynamic data				**Post-dilation hemodynamic data**			
Animal #	**Valve dilation #**	**RVp** (mmHg)	**PAp** (mmHg)	**ΔP** (mmHg)	**C.O** (L/min)	**RVp** (mmHg)	**PAp** (mmHg)	**ΔP** (mmHg)	**C.O** (L/min)
1	BD 1	47/6	18/9	29	2.3	48/5	22/9	26	2.8
	BD 2	28/5	18/8	10	2.6	23/5	18/8	5	2.6
	BD 3	18/0	15/4	3	2.5	16/2	12/4	4	2.5
	Term	18/9	16/10	2	3.5				
2	BD 1	38/3	15/5	23	3.2	31/0	19/6	12	3.6
	BD 2	32/5	19/9	13	4.1	32/6	19/7	13	5.2
	BD 3	22/5	12/6	10	3.2	17/3	12/7	5	4.2
	Term	20/2	14/5	6	2.6				
3	BD 1	33/2	14/6	19	2.9	32/5	26/8	6	3.5
	BD 2	24/2	16/8	8	5.1	27/4	16/11	11	6.4
	BD 3	24/10	17/11	7	2.8	22/7	14/10	8	3.8
	Term	21/9	20/13	1	3.4				
4	BD 1	41/9	20/18	21	3.1	34/12	19/15	15	3.9
	BD 2	43/2	21/13	22	5.4	40/9	23/19	17	7.5
	BD 3	25/5	16/9	9	4.3	28/5	17/8	11	5.5
	Term	33/3	15/12	18	6.2				
5	BD 1	28/1	8/5	20	4.2	24/2	15/4	9	4.6
	BD 2	42/9	16/11	26	5.1	36/6	19/10	17	7.6
	BD 3	25/3	14/6	11	5.2	28/2	14/6	14	6.5
	Term	29/0	19/10	10	5.7				
6	BD 1	22/4	12 / 5	10	3.2	23/2	13/3	10	3.4
	BD 2	30/0	15/9	15	3.2	33/0	23/14	10	3.3
	BD 3	25/0	16/10	9	4.6	22/0	13/10	9	5.2
	Term	27/0	13/7	8	5.9				
7	BD 1	33/0	10/5	23	3.3	31/1	13/6	18	3.6
	BD 2	32/5	17/9	15	3.9	37/4	20/13	17	4.5
	BD 3	29/0	13/9	16	4.7	24/0	13/5	11	5.1
	Term	30/3	17/7	13	5.9				

Echocardiography

Interval transthoracic echocardiography was performed to assess valve hemodynamic performance and overall heart function in the week prior to and following each scheduled balloon dilation procedure. During this procedure the animals received intramuscular injection of acepromazine (0.05 mg/kg) and butorphanol (0.2-0.4 mg/kg) for sedation. Animals were manually restrained and held in left lateral recumbency to allow for suitable imaging. 2-D echocardiography, including color and continuous wave Doppler imaging was used to assess valve function, including transvalvular flow velocity and transvalvular peak gradient (mmHg).

Table S7: **2-D echocardiogram derived transvalvular peak gradient at all valve expansion states.** The peak transvalvular gradient (mmHg) as measured by continuous wave doppler (CWD) is shown at each stage of valve expansion from 12.5 mm to 20 mm internal diameter (ID) in all 7 survival study animals throughout the 9-10 week survival period.

	Valve internal diameter (ID)			
Animal #	**12.5mm** Peak gradient (mmHg)	**16mm ID** Peak gradient (mmHg)	**18mm ID** Peak gradient (mmHg	**20mm ID** Peak gradient (mmHg)
1	17.8	5.5	7.8	11.2
2	36.3	14.4	20.5	14.1
3	22.4	17.7	14.4	13.5
4	25.6	24.4	17.9	15.7
5	22.3	16.5	19.9	12.9
6	12.9	13.3	10.8	12.4
7	18.1	20.6	13.1	13.2
Mean	22.2	16.1	14.9	13.3
Stdev	± 7.5	± 6.0	± 4.8	± 1.4

Fig. S15: Serial echocardiograms measuring transvalvular gradient in growing lambs. Representative 2-D transthoracic echocardiographic images demonstrating continuous wave Doppler measurement of peak transvalvular flow velocity at each state of device expansion during the 10-week survival period.

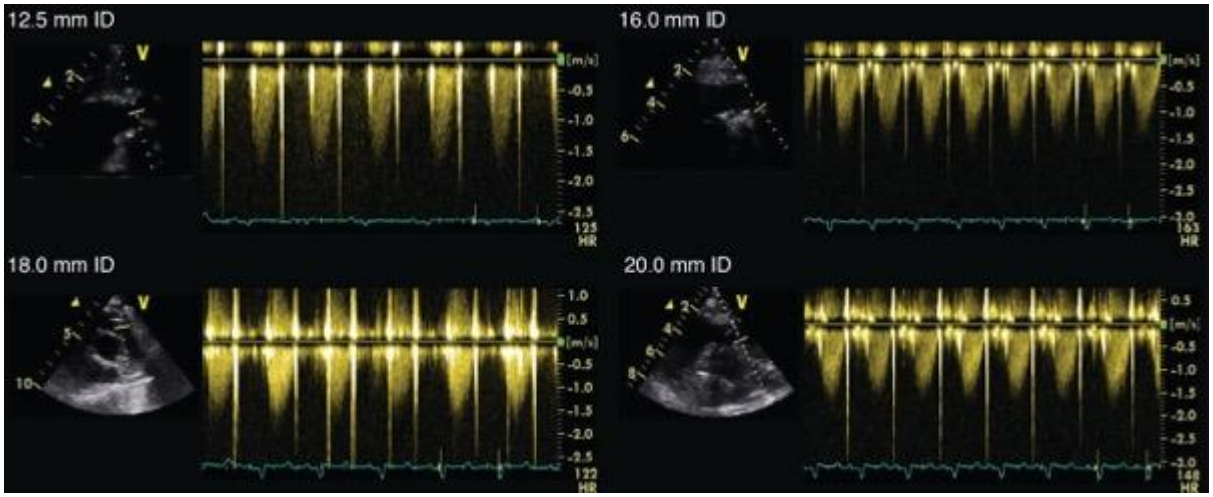

Term procedure

At the scheduled term date, animals were placed under anesthesia using the aforementioned regimen. Intracardiac hemodynamic measurements and angiographic imaging were obtained, as previously described. A right thoracotomy (4th intercostal space) incision was then performed to expose the heart. 2-D epicardial echocardiography (including color and continuous wave Doppler echocardiography) was performed to assess function of the valve device and overall heart function. After data collection, the animals were euthanized by intravenous injection of phenytoin/pentobarbital solution (Beuthanasia→-D, 87 mg/kg). Necropsy was performed for all study animals, with examination of the heart and valve implant. Gross pathological findings were also examined in the kidneys, lungs, brain, liver, spleen and gastrointestinal tract.

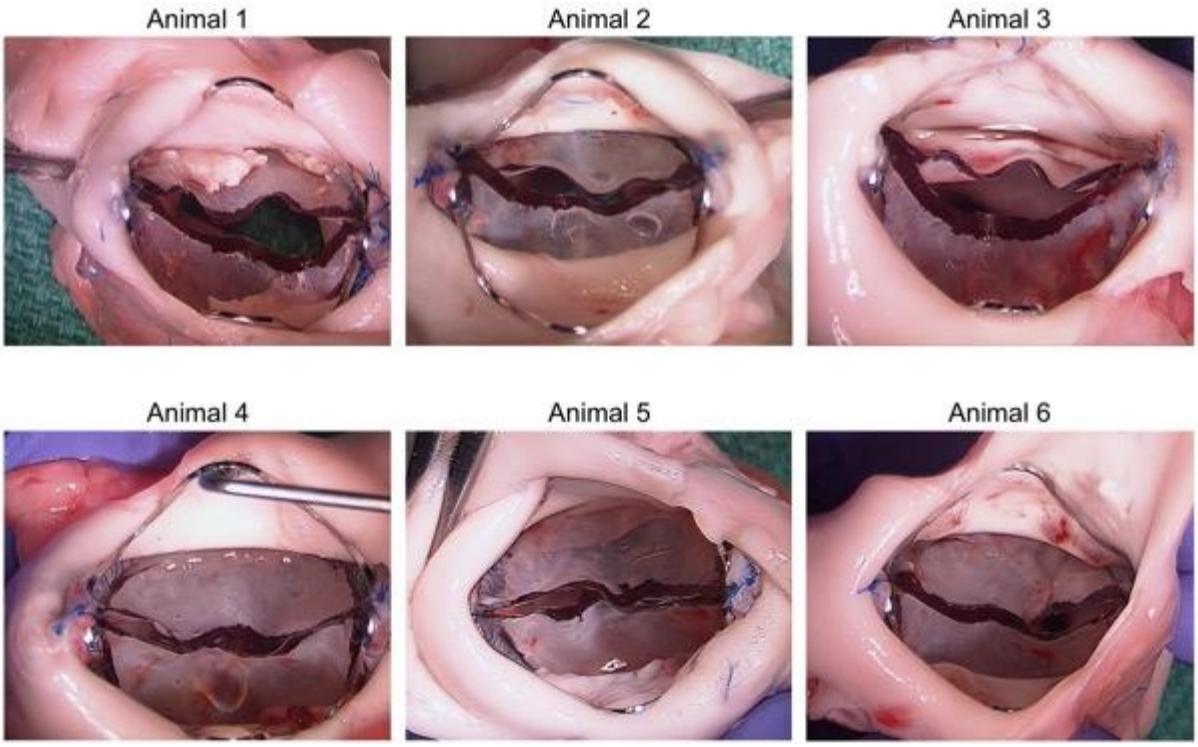

Fig. S16: Macroscopic appearance of biomimetic expandable valve at time of explant in 6 study animals. Images of valve outflow surface in six survival study animals at term procedure (9 - 10 weeks post implant). NB: Outflow view of study animal No. 7 is shown in the manuscript, Fig. 6A)

Histological analysis

Explanted valves and the attached pulmonary artery tissue were sent as block specimens (valve and adjacent pulmonary artery wall) for plastic processing and embedding. The device and surrounding tissue were dehydrated in a graded series of ethanol, then infiltrated and embedded in Spurr plastic resin. After polymerization, the device block was sectioned.

The specimen block was first sectioned longitudinally, as shown in Fig. 6B. This section was cut in the center of the valve, perpendicular to the free edge of the two leaflets. The longitudinal section was stained with Hematoxylin and Eosin and Miller's elastic stain.

Next, the valve was transversely sectioned, as shown in Fig. 6B. Sections were cut in the proximal, middle and distal segments of the valve. The proximal and mid sections incorporated the leaflet-frame attachment point at the valve base. The distal section incorporated the attachment point of the leaflets to the distal frame. The transverse sections were stained with Hematoxylin and eosin.

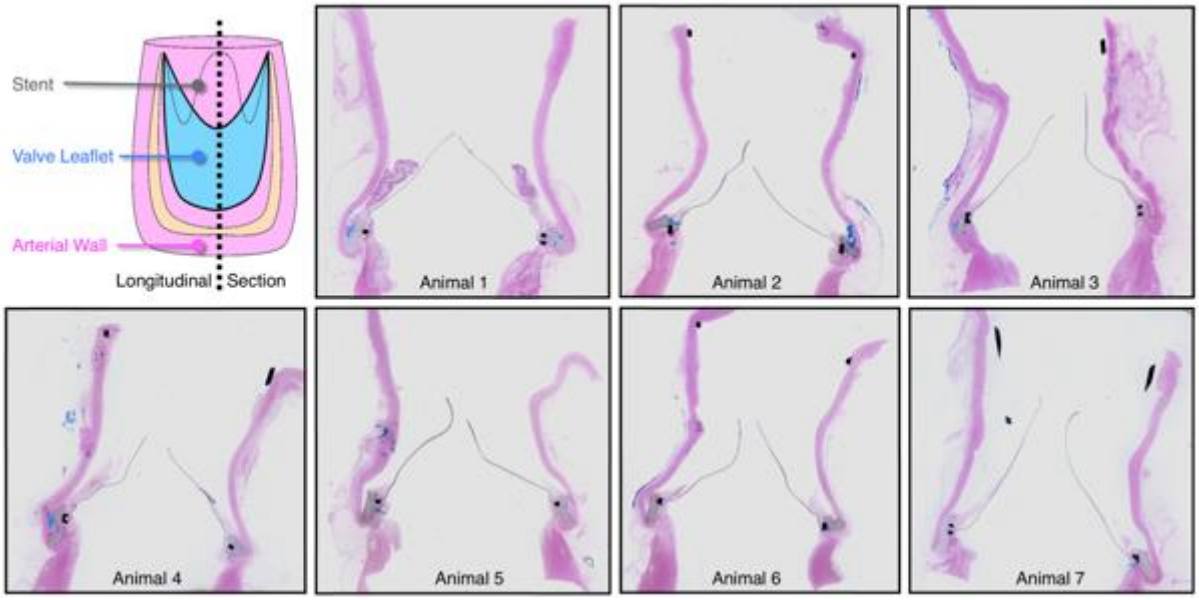

Fig. S17: Histological profile of biomimetic expandable valve prototype at time of explant (63-68 days post implantation). Hematoxylin and eosin (H&E) stained longitudinal sections of all 7 study animals. All images measure approximately 30mm in width.

Movie S1. A geometrically accommodating heart valve replacement. In this video, we demonstrate the venous-valve inspired biomimetic valve design using 3-dimensional models of the native human venous valve expanding under physiologic volume loads and its geometrically accommodating bileaflet valve analogue. We demonstrate functionality of the primary biomimetic valve design with footage of the expanding valve geometry in an *in vitro* flow loop system, and we show the results of finite element simulations evaluating the magnitude and distribution of stresses across the closed and loaded valve leaflet at various states of valve expansion. We present echocardiographic color Doppler images demonstrating laminar flow along the length of the valve and into the branch pulmonary arteries. Then, we demonstrate *in vivo* valve expansion in a growing animal, with representative footage of a balloon expansion procedure in a juvenile sheep at two weeks post valve implantation. This is followed by representative right ventricular angiograms performed at two- and seven-weeks post valve implantation, demonstrating successful valve expansion to accommodate growth. Finally, we provide echocardiographic (ultrasound) evidence of the biomimetic bileaflet valve flow dynamics obtained during acute and long-term *in vivo* studies, with representative epicardial echocardiogram color doppler images showing prominent flow recirculation around the valve periphery during the valve opening phase. This flow pattern we demonstrate on both short and long-axis echocardiographic views.